UC Irvine

UC Irvine Electronic Theses and Dissertations

Title

The mechanisms and casting parameters employed by Controlled Diffusion Solidification to reduce hot tearing susceptibility in wrought aluminum alloys

Permalink

https://escholarship.org/uc/item/7g56x50h

ISBN

9798171612818

Author

Small, Samuel

Publication Date

2023-10-26

Copyright Information

This work is made available under the terms of a Creative Commons Attribution License, available at https://creativecommons.org/licenses/by/4.0/

Peer reviewed|Thesis/dissertation

eScholarship.org Powered by the California Digital Library
University of California

UNIVERSITY OF CALIFORNIA,
IRVINE

The mechanisms and casting parameters employed by Controlled Diffusion Solidification to reduce hot tearing susceptibility in wrought aluminum alloys

THESIS

submitted in partial satisfaction of the requirements
for the degree of

MASTER OF SCIENCE

in Materials Science and Engineering

by

Samuel Small

Thesis Committee:
Professor Diran Apelian, Chair
Professor Lorenzo Valdevit
Professor Daniel R. Mumm

2023

© 2023 Samuel Small

TABLE OF CONTENTS

LIST OF FIGURES iv

LIST OF TABLES vii

ACKNOWLEDGEMENTS ix

ABSTRACT OF THE THESIS xi

Chapter 1: Introduction 1

Chapter 2: Background 3

2.1 Casting Wrought Aluminum Alloys 3

2.2 Controlled Diffusion Solidification 9

2.3 Alloy Systems 15

2.4 Processing Parameters 19

Chapter 3: Materials and Experimental Methods 24

3.1 Materials 24

3.2 Experimental Methods 25

3.2.1 Melting and Casting 25

3.2.1.1 Cooling Rate 28

4.1.1.1 Thermal Data 29

4.1.1.2 Effect of Varying T between Precursors (ΔT_P) 30

4.1.1.3 Effect of Mass Ratio and Mixing 31

4.1.1.4 Hot Tearing 31

4.1.2 Mold Design and Procedure 32

4.1.3 Materials Characterization 36

Chapter 4: Results and Discussion 39
4.1 Effect of Cooling Rate 39
4.1.1 Thermal Data 48
4.2 Effect of Varying T between Precursor Alloys (ΔT_P) 50
4.3 Effect of Mass Ratio and Mixing 59
4.3.1 Anomalous Grains 62
4.4 Hot Tearing 64
4.5 Castability 70
Chapter 5: Conclusions 72
Chapter 6: Future Work 75
References 76

LIST OF FIGURES

Figure 1: (a) Macroscopic image of hot tearing [8] and (b) diagram of hot tearing causes [2]..... 4

Figure 2: Effect of grain size and morphology on hot tearing severity in M206 [5]..... 5

Figure 3: Solute and temperature fields ahead of the S/L in conventional solidification..... 6

Figure 4: (a) Equiaxed dendrites growing toward each other and (b) solute fields of the dendrites impinging. 6

Figure 5: (a) Predominately dendritic microstructure and (b) predominately globular microstructure achieved by the addition of Al-5Ti-1B master alloy [12]. 7

Figure 6: (a) Diagram of rheocasting and of [21] (b) GISS [23]. 8

Figure 7: S+L Diffusion Solidification [25]. 10

Figure 8: Controlled Diffusion Solidification of Al-4.5%Cu and resultant microstructure [26].. 11

Figure 9: Growth in front of the solid liquid interface..... 13

Figure 10: Anomalous grain of pure Al (A) [43]..... 15

Figure 11: Chemical composition of 6061 [53]..... 18

Figure 12: Effect of cooling rate on microstructures produced by CDS [35]..... 20

Figure 13: Effect of superheating the HTM on microstructures produced by CDS [35]. 20

Figure 14: Simultaneous mixing apparatus for CDS [2]. 22

Figure 15: Simultaneous mixing [2]. 22

Figure 16: (a) Box furnaces and (b) graphite crucibles used for melting. 26

Figure 17: Framework for all CDS experiments..... 28

Figure 18: (a-b) Graphite mold and casting produced from it and (c-d) steel mold and casting produced from it..... 33

Figure 19: (a) Hot tearing sand mold, (b) sprue piece, and (c) both mold and sprue in action. ... 35

Figure 20: Tensile bar permanent mold with precast insert. 36
Figure 21: Location of samples taken from clay graphite mold castings. 36
Figure 22: OES spark locations for (a) graphite cast samples and (b) sand mold samples. 37
Figure 23: Visual representation of circularity [60]. 38
Figure 24: Anodized microstructure of Al-4.5%Cu cast by (a)-(b) conventional solidification and (c)-(d) Diffusion Solidification with cooling rates of (a)(c) 0.2 ℃/s and (b)(d) 12.8 ℃/s, and the effect of cooling rate on grain size and grain circularity in (e) conventional and (f) Diffusion Solidification castings. 40
Figure 25: Anodized microstructure of AA6061 cast by (a)-(b) conventional solidification and (c)-(d) Diffusion Solidification with cooling rates of (a)(c) 0.2 ℃/s and (b)(d) 12.8 ℃/s, and the effect of cooling rate on grain size and grain circularity in (e) conventional and (f) Diffusion Solidification castings. 44
Figure 26: Thermal curves obtained during the mixing step of CDS of Al-4.5%Cu. 48
Figure 27: Thermal curves obtained during the mixing step of CDS of 6061. 49
Figure 28: Anodized microstructure of Al-4.5%Cu cast by CDS with a mass ratio of 4:1 and a ΔT_P of (a) 0°C, (b) 66°C, (c) 80°C, and (d) 95°C between precursor alloys accompanied by (e) effect of the variance of ΔT_P on morphology. 51
Figure 29: Anodized microstructure of 6061 cast by CDS with a ΔT_P of (a) 0°C, (b) 55°C, and (c) 71°C between precursor alloys accompanied by (d) the effect of variance of ΔT_P on morphology. 54
Figure 30: Comparison of (a) Al-4.5%Cu cast by conventional solidification against (b) CDS with a ΔT_P of 0°C and (c) 6061 cast by conventional solidification against (d) CDS with a ΔT_P of 0°C accompanied by (e) corresponding grain statistics. 56

Figure 31: Comparison of AA6061 cast by Diffusion Solidification with a ΔT_P of 0°C both (a) without Cr and (b) with Cr accompanied by (c) corresponding grain statistics. 58
Figure 32: Microstructures of Al-4.5%Cu cast by CDS with mass ratios of (a) 6.33:1 and (b) 4:1 with (c) graphical representation of the contrast in morphology. 60
Figure 33: Effect of mass ratio and ΔT_P on mixing efficiency. 61
Figure 34: (a-b) Optical micrographs of an anomalous grains, (c) backscatter electron (BSE) image of the grain, and (d) EDS line scan of the grain. 63
Figure 35: Hot tearing tests of 6061 cast in sand molds conventionally and by CDS. 65
Figure 36: Microstructures (a) Conv. 1 and (b) CDS 1 hot tearing tests. 68
Figure 37: Conventionally and CDS cast 6061 hot tearing tests in a permanent tensile bar mold. Hot tears are indicated by red arrows, cold shuts by blue. 69
Figure 38: CDS castings of 6061 with significant pouring defects. 71

LIST OF TABLES

Table 1: List of CDS experiments run to date [52]. 17

Table 2: Master alloys used to create precursor alloy compositions. 24

Table 3: Precursor alloys used in casting experiments. 24

Table 4: Varying the cooling rate of Al-4.5%Cu castings. 28

Table 5: Varying the cooling rate of 6061 castings. 29

Table 6: Parameters used to obtain thermal curves during the mixing step of CDS. 30

Table 7: Al-4.5%Cu parameters varying the temperature between precursor alloys (ΔT_P). 31

Table 8: 6061 parameters varying the temperature between precursor alloys (ΔT_P). 31

Table 9: Al-4.5%Cu experimental parameters varying the mass ratio between precursor alloys. 31

Table 10: 6061 experimental parameters testing hot tearing susceptibility. 32

Table 11: Tabulated effects of cooling rate on grain size and circularity in Al-4.5%Cu cast conventionally and by CDS. 41

Table 12: Tabulated effects of cooling rate on grain size and circularity in 6061 cast conventionally and by CDS. 45

Table 13: Effect of cooling rate on both Al-4.5%Cu and 6061. 47

Table 14: Effect of differences in ΔT_P on grain morphology in Al-4.5%Cu 50

Table 15: Effect of differences in ΔT between precursor alloys on grain morphology in 6061. . 55

Table 16: Conventional vs CDS with $\Delta T_P = 0°C$. 57

Table 17: Effect of Cr in the HTM. 58

Table 18: Effect of mass ratio on grain size and morphology. 60

Table 19: Effect of ΔT_P on mixing efficiency in CDS of 6061 61

Table 20: Effect of solid preformed in the LTM on mixing efficiency. 62

Table 21: Measured compositions of 6061 hot tearing castings in sand molds..... 66

Table 22: Hot tearing results listed from most severe hot tearing to least..... 67

Table 23: Hot tearing and casting defects in 6061 cast conventionally and by CDS. 68

ACKNOWLEDGEMENTS

I would like to express my sincere appreciation to my advisor, Dr. Diran Apelian. Under his guidance, I was able to grow as a researcher, a professional, and person. The lessons were not always easy, but they were, invariably, worth learning.

I would also like to thank Dr. Carl Söderhjelm for helping make this thesis a reality. Without his help and his time, none of this would have been possible. Further, his guidance on life after graduate school was invaluable.

A huge thank you is due to my committee members, Dr. Daniel Mumm and Dr. Lorenzo Valdevit. Their teachings, mentorship, and time investment will never be forgotten.

Shri, Raquel, Cheolmin, Taiki, Calvin, and Sakshi were always there to support and encourage me. They also helped me immensely when it came time to run experiments and train on equipment. I will miss them all dearly.

Dr. Benjamin MacDonald was always a fantastic resource for both research and presentation advice. He and Calvin helped both helped me enormously in my hunt for jobs after graduate school.

Monica has been a constant source of joy and support from the moment that I met her. She was a rock that I could always count on for encouragement when times were difficult. I could not have done this without her and her family.

Finally, I would like to thank my family and my friends, especially my parents, for their unfaltering support over the course of my entire life leading up to this moment and, hopefully,

well past it. I hope one day that I can repay the immense debt of gratitude that I owe to each and every one of them.

ABSTRACT OF THE THESIS

The mechanisms and casting parameters employed by Controlled Diffusion Solidification to reduce hot tearing susceptibility in wrought aluminum alloys

by

Samuel Small

Master of Science in Materials Science and Engineering

University of California, Irvine, 2023

Professor Diran Apelian, Chair

This study investigates the efficacy of Controlled Diffusion Solidification (CDS) in refining grain structure and improving castability in Al-4.5%Cu and 6061 alloys. Experimental results demonstrate that CDS, in combination with high cooling rates, produces smaller grains than either method alone with only minor reductions in the globular morphology, challenging existing theories on globular grain growth. Chromium additives further refine the grain structure, suggesting avenues to improve fluidity in 6061 cast by CDS. The study also reveals limitations in existing mixing methods, calling for improved techniques for solute homogenization.

Hot tearing tests on are conducted on 6061 cast by CDS. Castability is influenced by both hot tearing susceptibility and fluidity; CDS excels in reducing the former but compromises the latter. High-pressure die casting emerges as the most suitable casting process for CDS, consistent with other semi-solid metal processes.

Finally, a new mechanistic framework is proposed to explain CDS's role in grain refinement. The framework considers nucleation dynamics, thermal and chemical equilibration, and solute field impingement, culminating in a globular microstructure. This study serves as a

foundation for optimizing CDS for industrial applications, while also highlighting areas that require further research.

Chapter 1: Introduction

Controlled Diffusion Solidification (CDS) is a semi-solid metal casting (SSM) process with potential applications in casting wrought aluminum alloys. It is known for producing globular microstructures in alloys that are typically dendritic, thereby reducing their susceptibility to hot tearing. Despite its potential advantages, the mechanisms underlying the formation and growth of globular microstructures and their direct influence on hot tearing are not yet fully understood.

This work addresses three crucial objectives to advance the CDS process toward industrial scalability. The first objective is to clarify the mechanisms responsible for the formation of globular microstructures. A better understanding of the fundamentals is imperative if improvements are to be made. The second objective involves evaluating the suitability of CDS for various casting methods, including sand casting, permanent mold gravity casting, and high-pressure die casting (HPDC). Existing research has not thoroughly explored how process parameters—such as cooling rate, mixing temperature, and mixing rate—might impact the success of CDS. The final objective is to consider hot tearing and melt fluidity, two crucial impediments to casting complex geometries.

To this point, experimental studies on CDS have been relatively small in scale, with the largest castings weighing only up to 4 kg [1][2]. A comprehensive understanding of how various process parameters affect both the microstructure and the severity of hot tearing is indispensable for scaling CDS to industrial applications. Moreover, while the notion that a finer, globular microstructure minimizes hot tearing is generally accepted, it remains an open question whether the mechanisms in CDS are consistent with those in traditional casting methods for wrought aluminum alloys.

To tackle the first and second objectives of clarifying the mechanisms contributing to the formation of globular microstructures within CDS and identify suitable casting methods, a comprehensive exploration of the cooling rates, controlled temperature variances, and mass ratios between the mixed alloys during CDS will be carried out. The observations from these experimental manipulations are anticipated to provide a deeper understanding of the fundamental principles governing microstructure formation within CDS, which is essential for deriving strategies to refine the process further.

Regarding the final objective, an observation of the hot tearing susceptibility and melt fluidity issues inherent to CDS castings will be conducted, particularly when dealing with complex geometries. Concurrently, an assessment of melt fluidity and its implications on casting complex geometries will be undertaken. These investigations are primed to provide a more elaborate understanding of the challenges and possible mitigations concerning hot tearing and melt fluidity in CDS. Moreover, they will facilitate a comparative analysis to ascertain whether the mechanisms observed in CDS align with those in traditional casting methods for wrought aluminum alloys.

In conclusion, the methodological blueprint of this thesis is structured to not only delve into the underlying mechanics of the CDS process but also to evaluate its adaptability across different casting processes and discern its benefits and challenges in relation to hot tearing and melt fluidity. Through an examination of each objective, this thesis aims to propel the CDS process closer to industrial scalability.

Chapter 2: Background

2.1 Casting Wrought Aluminum Alloys

Casting processes offer numerous advantages over wrought methods in aluminum production. These benefits range from the capacity to craft complex geometries that are unachievable with wrought techniques, to producing near-net shapes that minimize waste, and to eliminating the need for expensive, time-consuming machining. However, despite these advantages, wrought products still dominate, constituting 75-80% of global aluminum production [3]. The primary reason for this is clear: the aluminum alloys with the most desirable characteristics cannot be cast. Aluminum alloys fall into two main categories—those that are suitable for casting (cast alloys) and those that are not (wrought alloys). Wrought alloys benefit from a more expansive design space to optimize properties because they are not constrained by castability. To extend the advantages of casting to wrought alloys, two impediments must be overcome: bad fluidity, which will be addressed later, and susceptibility to hot tearing.

Hot tearing, also called hot cracking or solidification cracking, is the formation and propagation of cracks during solidification of susceptible alloys. These cracks can range in severity from microscopic to catastrophic, as shown in Figure 1, and invariably lead to reduced properties. The cause of hot tearing is complex and multiple theories have been adapted to explain it, but there are some objective truths. One of which is that hot tearing occurs in the semi-solid state of solidification [4]. The reasons for this are contrived, some theories stating that shrinkage porosity forms stress concentrations where interdendritic liquid is unable to feed it through coherent dendritic network [5]. Other theories state that hot tears are simply due to uniaxial tensile failure in the weak portions of the casting [6]. One other theory suggests that hot

cracks form in the interdendritic liquid in the form of a liquid film, again due to lack of feeding [7].

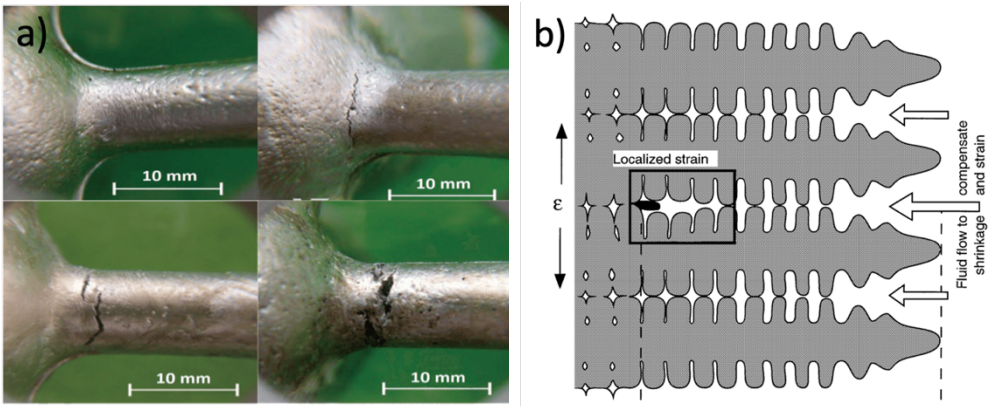


Figure 1: (a) Macroscopic image of hot tearing [8] and (b) diagram of hot tearing causes [2].

Regardless of the underlying cause, the consensus is that hot tearing can be alleviated through two primary means: reducing grain size and achieving a more globular, or spherical, morphology, as illustrated in Figure 2 [5]. The rationale behind this is that smaller grains experience reduced strain, allowing the interdendritic liquid to better fill any emerging shrinkage porosity and cracks. In essence, the key to mitigating hot tear susceptibility lies in limiting dendritic growth.

In conventional solidification processes, dendrites start forming when a small perturbation appears in the planar solidification front. Due to non-equilibrium conditions during solidification, solute is pushed out both in front of and to the sides of this perturbation, which causes a level of undercooling ahead of the advancing solidification front, as depicted in Figure 3 [10][11]. This solute field enrichment and the resulting undercooling are fundamental drivers for dendritic growth.

However, if there is a high enough density of equiaxed dendritic grains, the solute fields from two or more neighboring grains would impinge, as shown in Figure 4. This impingement

negates the solute gradient in front of the solid-liquid interface (S/L), thereby eliminating the driving force for constitutional undercooling and leaving only the driving force for curvature undercooling [12][13]. Curvature undercooling then acts to flatten the dendrite tip and revert the S/L interface to planar growth. The outcome is a formation of small grains that exhibit globular morphologies.

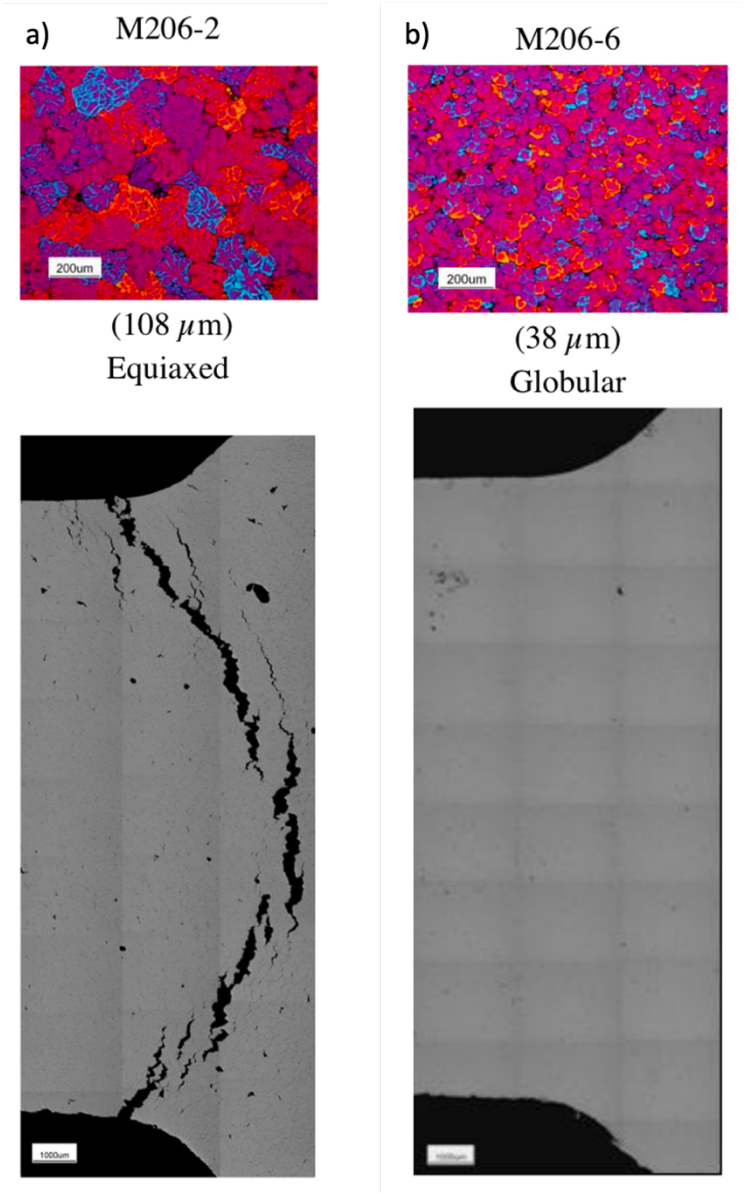


Figure 2: Effect of grain size and morphology on hot tearing severity in M206 [5].

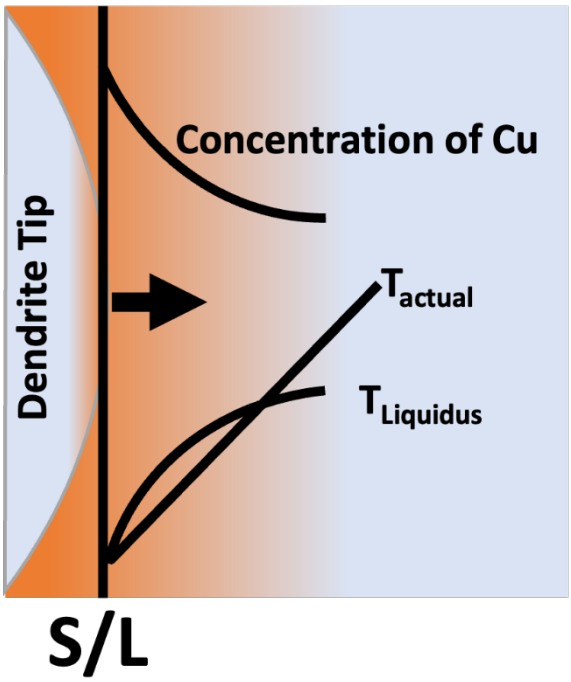


Figure 3: Solute and temperature fields ahead of the S/L in conventional solidification.

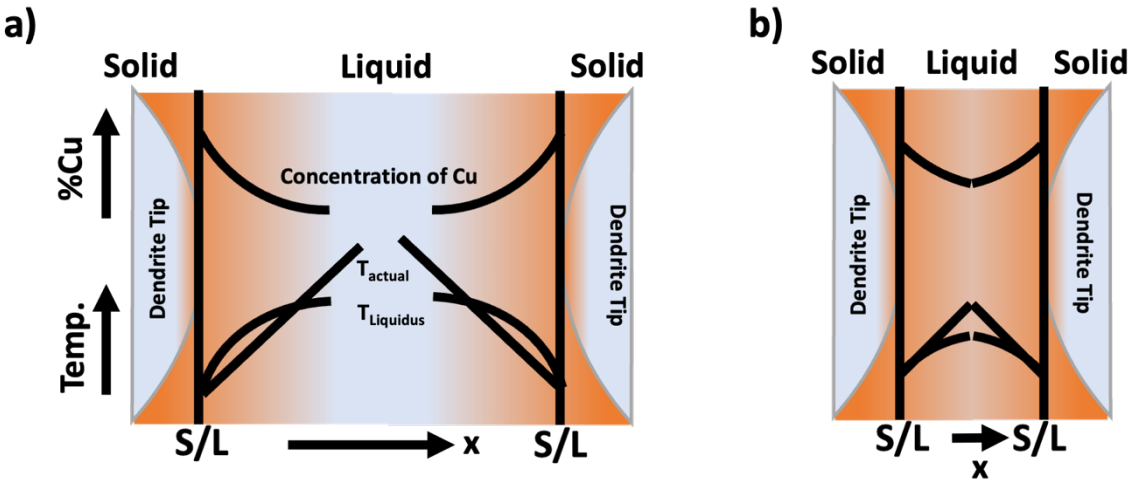


Figure 4: (a) Equiaxed dendrites growing toward each other and (b) solute fields of the dendrites impinging.

The key to casting wrought aluminum alloys, then, is high grain density, which can be achieved by grain refinement, also known as grain multiplication. There are several casting

processes that produce refined grains of globular morphology by different means, and each comes with unique challenges.

A common method of grain refinement is the use of inoculants like titanium diboride (TiB_2) and Cr to induce copious nucleation. Even so, there are many questions regarding the scientific understanding of how these inoculants nucleate so many grains. One understanding is that inoculant particles like TiB_2 act as sites for heterogeneous nucleation [12][14] [15]. Another suggests that solute elements like Cr or Ti induce icosahedral short-range ordering to form quasicrystals that nucleate FCC Al by heteroepitaxy [16]. Cr additions to Al-Zn alloys and pure Al have been shown to affect excellent grain refinement, but solute poisoning occurs with the addition of other alloying elements like Mg and Si [17][18][19]. Regardless of the mechanism, grain refiners reduce grain size and increase shape factor, as shown in Figure 5, by copious nucleation of grains. Grain refiners can, however, introduce inclusions that may be undesirable for extrusion or structural applications [14], so other options have been explored.

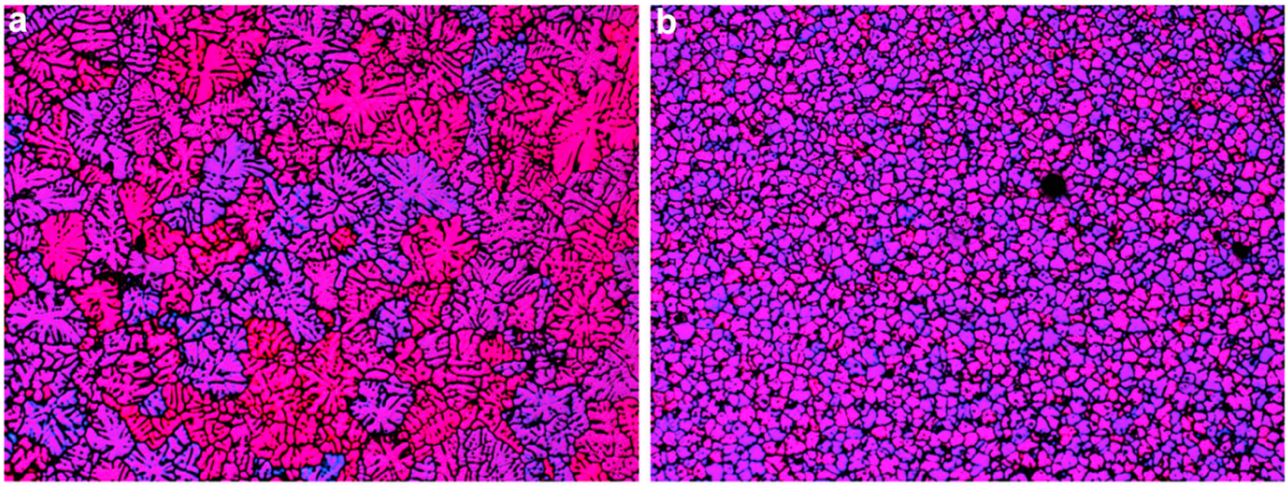


Figure 5: (a) Predominately dendritic microstructure and (b) predominately globular microstructure achieved by the addition of Al-5Ti-1B master alloy [12].

Semi-solid metal (SSM) processes manipulate aluminum melts while in the semisolid state. Rheocasting, which is shown in Figure 6a, and thixoforming apply shear forces by

convection to semisolid slurries that breaks off dendrite arms as they form [20][21]. Ultrasonic grain refinement operates on the same principle as rheocasting and thixoforming but utilizes ultrasonic vibrations induce convection [22]. Gas-induced semi-solid processing (GISS) induces convection by flow of numerous tiny gas bubbles into a semi-solid slurry, which is illustrated in Figure 6b [23]. Regardless of the method, the result is an inhibition of long-range dendritic growth as well as copious heterogenous nucleation upon free floating fragmented dendrites. Globular grains are achieved by inducing a high grain density.

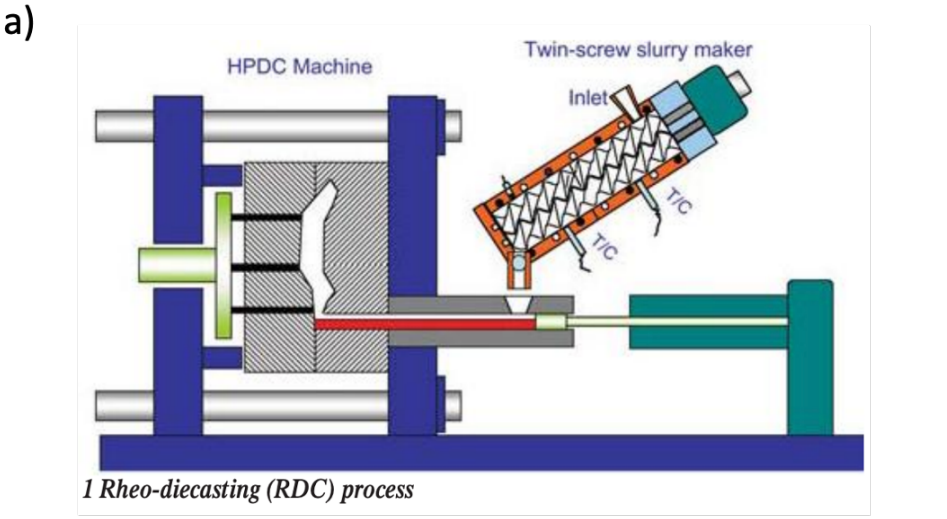


Figure 6: (a) Diagram of rheocasting and of [21] (b) GISS [23].

2.2 Controlled Diffusion Solidification

Controlled Diffusion Solidification is a SSM aimed directly at casting wrought alloys without hot tearing. It achieves this in much the same way as other SSMs: smaller grains with a globular morphology. However, the mechanisms that produce castings with these grains are unclear, and the current understanding is very different from the other methods of grain refinement.

Diffusion Solidification was developed as a precursor to CDS with the aim of reducing the casting temperature for steel. This makes it possible to use a wider variety of molds that can withstand lower temperatures. In this isothermal process, a liquid is introduced into a solid powder; both having unique chemical compositions. When they reach an equilibrium state, the overall composition falls within the solid region of the phase diagram, as shown in Figure 7 using carbon steel as an example [24][25]. Unlike traditional casting methods, which are dominated by heat flow, Diffusion Solidification is driven by mass flow.

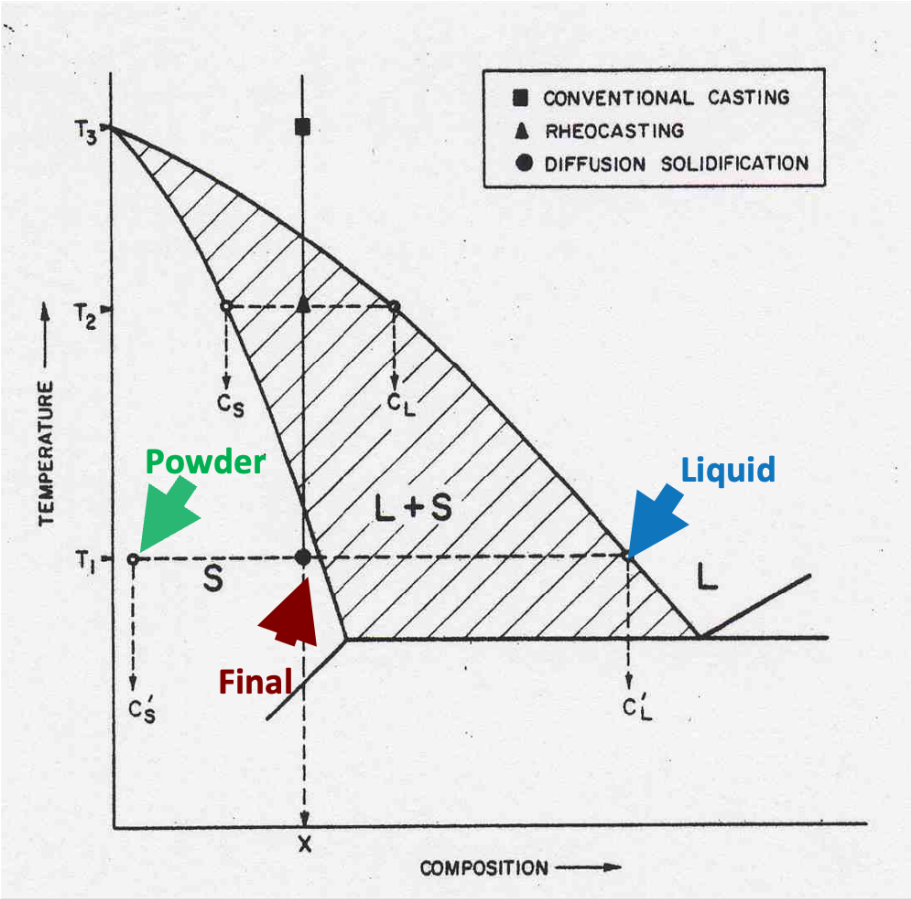


Figure 7: S+L Diffusion Solidification [25].

Controlled Diffusion Solidification, as it is currently understood, operates on a similar defining principle. CDS is a semi-solid metal process in which two precursor alloys with controlled composition and temperatures slightly above their respective liquidus are combined by some form of mixing. The fundamentals of CDS are represented in an example experiment in Figure 8. The result is a third alloy of a chosen composition with globular grains, also shown in Figure 8. Upon mixing of the precursor alloys, thermal equilibration, mass equilibration, solidification, and mechanical mixing occur concurrently. Like Diffusion Solidification, heat flow is no longer the dominate, but rather one of several driving factors for solidification behavior.

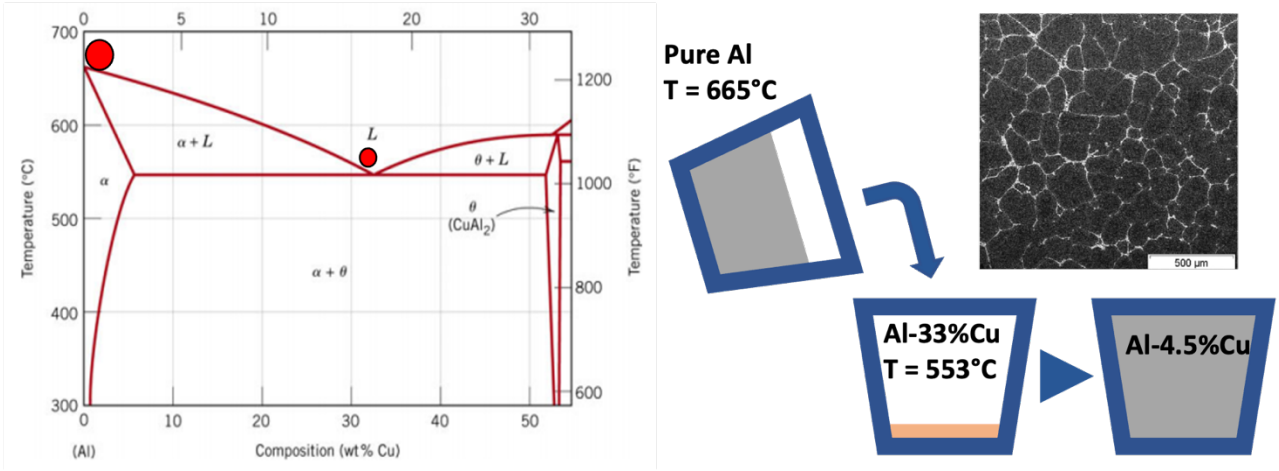


Figure 8: Controlled Diffusion Solidification of Al-4.5%Cu and resultant microstructure [26].

Understanding of the process has naturally evolved since it was introduced in the early 2000s. During that time, three mechanisms have been proposed to explain the growth of globular grains. Each of them depends upon a difference between chemical and thermal equilibration. This allows undercooling of HTM to allow heterogeneous nucleation directly upon mixing. Prandtl number is a dimensionless number that defines ratio of momentum diffusivity to thermal diffusivity [27]. It is written as:

(1)

where μ is dynamic viscosity, C_p is specific heat capacity, and k is thermal conductivity. Momentum diffusivity precedes chemical diffusivity, so if Prandtl number is below 1, thermal equilibration will occur before chemical. Typical Al alloy melts have viscosities ranging from 0.8 to 1.2 MPa·s [28], specific heat capacities ranging from 1.1 to 1.9 J/gK [29], and thermal conductivities ranging from 60 to 160 W/mK [30]. Given nominal values, Pr is 0.0125, meaning that thermal diffusivity is 80 times the value of momentum diffusivity. Even the worst case given

the ranges, thermal diffusivity is approximately 20 times higher than momentum diffusivity. In other words, the assumption that mass equilibration occurs after thermal equilibration is reasonable. Note that all mechanistic theories are founded and tested in the Al-Cu binary system.

The first mechanistic framework was published by Apelian et al. in 2006 [26][31] and can be parceled into three considerations: two involving nucleation and one involving growth. The first consideration is based on work by Cini et al. showing that energy barrier to nucleation is reduced if

(2)

where σ^{SL} is the interfacial energy between a solid of composition C_0 and σ_A^{SL} is the interfacial energy between the liquid precursor alloys [32]. The second consideration is that the free energy of the precursor alloys prior to mixing – including the ~5°C superheat – should be lower than the free energy of the resultant liquid *at its liquidus*. The final consideration is that, once the grains have nucleated, convection will be sufficient to deplete the boundary layer ahead of the S/L and stabilize it [33][34]. In other words, upon mixing the precursors together, a diffuse boundary will form with pockets of one precursor in the other. This diffuse boundary will act as a nucleation site as thermal equilibration happens and before chemical equilibration happens. The nuclei formed will grow with a planar front due to convective and mixing currents, resulting in globular grains. However, the work of Das et al. and Wu et al. suggest that the convective currents must be maintained throughout a significant portion of solidification to affect a globular microstructure, and it seems unlikely that CDS fulfills that condition.

The next mechanism, first proposed by Apelian and Saha in 2005 before evidently losing favor to the previous mechanism, resurfaced in 2007 in work by Symeonidis et al. [35][36][37]. This mechanism assumes the same nucleation theory as the previous but differs in the growth mechanism. It states that nuclei that form at the interface *prior* to full thermal equilibration will survive only if they then are carried by mixing currents into the low temperature precursor (LTM). The high concentration of solute around the nuclei will stabilize the S/L by disallowing constitutional undercooling in front. Figure 9 demonstrates the difference in solute fields between conventional solidification and CDS.

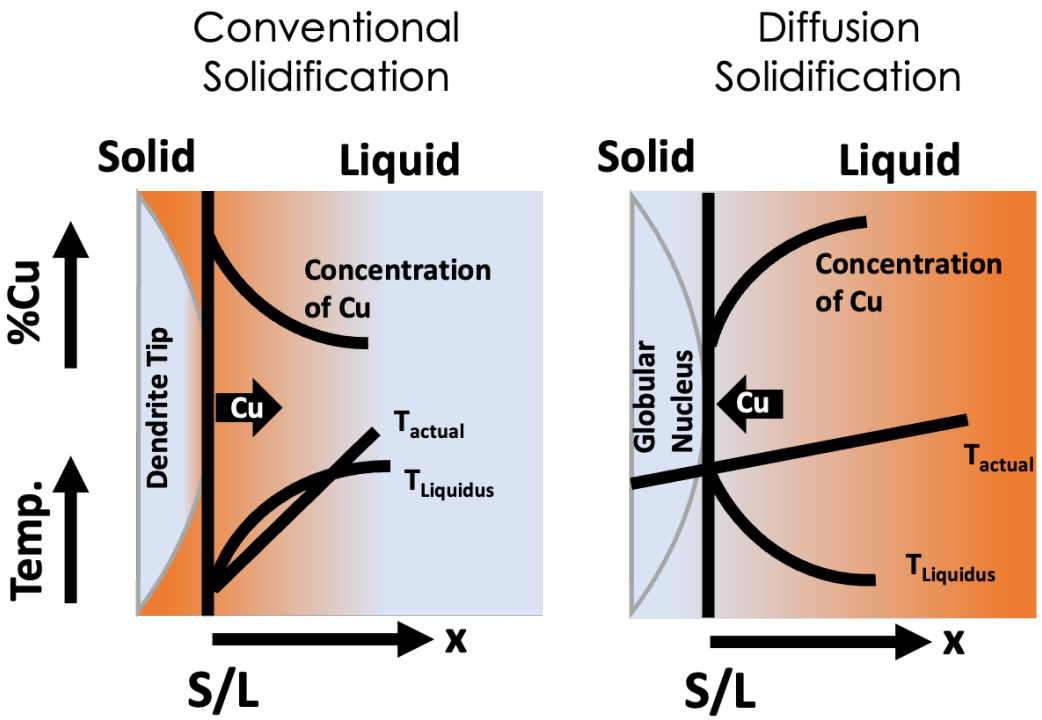


Figure 9: Growth in front of the solid liquid interface.

The most recent understanding was first proposed by Khalaf et al. in 2009 [38][39]. Figure 10a shows a theoretical thermal curve of the mixing step of CDS. The curve is segmented into essentially three sections: segment AB, segment BCD, and segment DE. Khalaf et al. suggest that segment AB accounts for the formation of the large anomalous grains marked “A”

in Figure 10b, segment BCD accounts for the globular regions marked “B”, and segment DE accounts for the dendritic regions marked “C”. The anomalous “A” grains are primarily pure Al, as shown in the line scan in Figure 10c. It is suggested that these grains nucleate and solidify before chemical or thermal equilibrium are reached due to copious nucleation of large pockets of pure Al. These grains were studied at length by Khalaf et al., and they were found to account for less volume with increased mixing rate [40][41][42][43]. The globular “B” regions more commonly associated with CDS are said to nucleate in convective hexagonal cells of pure Al surrounded by Al-Cu. These nuclei are then said to grow outward toward high the high solute walls of the convective cells with solute traveling toward the S/L as shown in the right schematic of Figure 9. The final dendritic “C” regions are said to nucleate and grow in the leftover liquid after thermal and chemical equilibration are reached. While this is the most recent mechanistic understanding, it is not well supported by evidence and there are still questions about exactly where the nucleation is occurring in each of these steps.

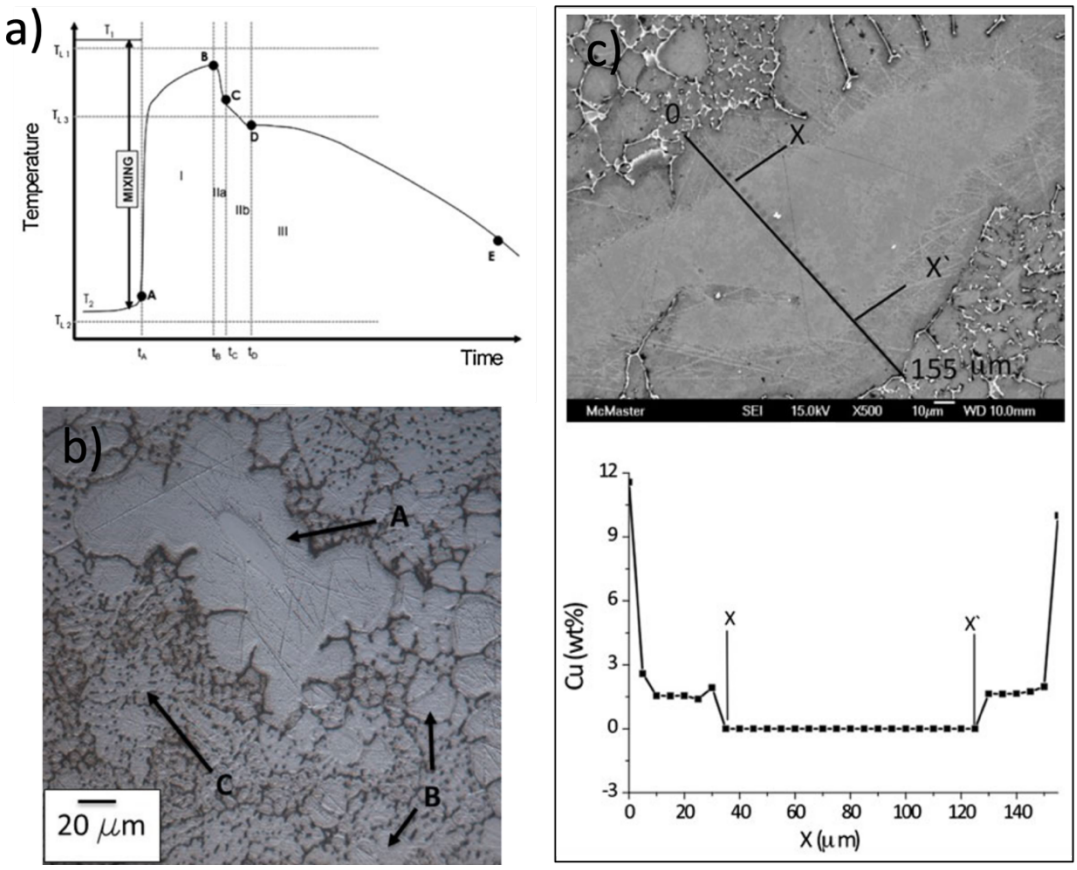


Figure 10: Anomalous grain of pure Al (A) [43].

In summary, although every other SSM, not to mention grain refiners, utilizes grain multiplication to increase grain density and produce globular microstructure, the proposed mechanisms for CDS suggest that it breaks convention. The first two mechanisms suggest copious nucleation, the primary mechanism of grain refiners, but suggest different growth mechanisms. There are still a lot of questions to be answered mechanistically, not the least of which is whether the mechanism could simply be copious nucleation and solute field impingement.

2.3 Alloy Systems

As mentioned previously, all the current mechanistic theories are grounded in the Al-Cu binary system, while many of the feasibility studies listed in Table 1 have multiple solute

elements with no update to the underlying theory. In the table HTM refers to high thermal mass and LTM refers to low thermal mass. TL1 is the liquidus of the HTM and TL2 is the liquidus of the LTM. All the non-binary alloys listed in Table 1 were feasibility studies except for the alloy poured by Pourgharibshahi et al., who attempted to clarify nucleation events in a 7068 alloy [44]. Success in feasibility tests hinged predominately on the microstructure, wherein relatively small and globular grains indicated said success. Ghiaasiaan et al. cast tensile bars of 7xxx series to obtain tensile data with mixed results [1][45]. Symeonidis and Khalaf used the Al-Cu binary system to test the effect of process parameters such as cooling rate and mixing rate on the size and shape of grain morphology in CDS [36][46], while Yang used the Al-Si binary system to further test mixing rate [47].

Table 1: List of CDS experiments run to date [52].

Alloy Designation	*HTM Precursor Alloy*	*LTM Precursor Alloy*	*TL1*	*TL2*	*T1*	*T2*	*Mass Ratio*	*Reference*
2014	Pure Al	Al-33Cu	660	548	665	550	6	[26][43]
	Pure Al	Al-36.7Cu-6.6Si-4.3Mg	660	562	665	567	7	[35]
2024	Al-I.5Mg	Al-33Cu-1.5Mg	651	543	653	548	6	[48]
4044	Pure Al	Al-12Si	660	580	665	585	1/2	[2]
4145	Al-12.7Si	Al-33Cu	578	548	585	550	6	[26]
5056	Pure Al	Al-35Mg	660.7	451	665	445	6	[26]
6082	Al-I.2Mn	Al-6.6Mg-7.7Si	659	604	668	604	10	[48][49]
7050	Al-7Zn-2.65Mg	Al-24Cu	634	589	640	592	9	[50]
	Al-267Mg-2.5Cu	Al-42.5Zn	641	602	646	615	6	[42]
	Al-2.8Mg	Al-23.8Zn-8.68Cu	645	580	655	610	3	[45]
7075	Al-3Mg	Al-36Zn-16Cu	644	520	647	534	6	[48]
	Pure Al	Al-11.2Zn-5Mg-3Cu	660	607	660	620		[47]
7068	Al-3.47Mg	Al-7.8Zn-2.6Mg-8Cu	642	647	575	580	3	[44]
7xxx	Al-I.33Mg	Al-18Zn	652	630	660	635	3	[51]
	Al-2.87Mg	Al-18Zn	641	630	650	630		
	Al-2.87Mg	Al-24Zn	641	618	650	625		
	Al-2.87Mg	Al-30Zn	641	608	650	612		
	Al-2.87Mg	Al-18Zn-6Cu	641	612	650	620		
	Al-2.67Mg	Al-22Zn-4Cu	645	607	650	615		
	Al-2.8Mg	Al-23.6Zn-4.9Cu	641	608	650	615		
	Al-3.47Mg	Al-31.2Zn-8Cu	641	570	650	600		
222	Pure Al	Al-33Cu	660	543	665	552	3	[26]
319	Al-7Si	Al-33Cu	-	543	620	552	7	[26]
206	Al-2.6Mg-2.4Mn	Al-33Cu	-	543			6	[35]

There are a few criteria one should consider when selecting suitable alloys for casting by CDS. The first, most obvious criterion is hot tearing susceptibility. If it does not hot tear, it should probably be cast conventionally. The second is dependent upon the strengthening mechanism. Alloys strengthened by strain hardening are not suitable candidates for casting via CDS or casting at all for that matter. Lastly, it should be a useful alloy with desirable properties.

Al-4.5%Cu is a suitable alloy for casting by CDS. The main strengthening mechanism in Al-4.5%Cu is precipitation hardening, which requires no deformation of the casting. It also

represents a series of alloys with very high strength, the 2xxx series. One of the most popular 2xxx series alloys, 2014, is Al-4.4%Cu with small additions of Si, Mn, and Mg. Even A206, a casting alloy with 4.5%Cu and other additions, has issues with hot tearing. Finally, the mechanisms of CDS are derived from Al-4.5%Cu. It is the perfect system to benchmark success in CDS and confirm the effect process parameters have on the microstructure.

6061, the composition of which is shown in Figure 11, is another prime candidate for CDS. It adds the complexity of multiple solute elements, has excellent mechanical and corrosion properties, hot tears easily, and is precipitation hardened. It is also one of the most popular aluminum alloys produced. Finally, Cr, if placed in the HTM, could act as a grain refiner [16][44].

Component	Wt. %	Component	Wt. %	Component	Wt. %
Al	95.8 - 98.6	Mg	0.8 - 1.2	Si	0.4 - 0.8
Cr	0.04 - 0.35	Mn	Max 0.15	Ti	Max 0.15
Cu	0.15 - 0.4	Other, each	Max 0.05	Zn	Max 0.25
Fe	Max 0.7	Other, total	Max 0.15		

Figure 11: Chemical composition of 6061 [53].

These two alloy systems will be considered in this work for the reasons listed above. Al-Cu results will be compared to previous work to verify success and benchmark best practices. It will also be used to test the effect of certain parameters that will be discussed in the next section. Once the benchmark has been set in Al-Cu, 6061 will also be used to test many of the same parameters. Finally, since 6061 has not yet been reportedly cast by CDS, a feasibility study will be carried out.

2.4 Processing Parameters

Successful castings by CDS thus far have been determined by the size and the shape of the grains. As it is with other grain refining techniques, small and globular grains are the marks of success. It is important, then, to observe *quantitatively* what processing parameters can change morphology during CDS and in what way. In this way, optimum conditions and suitable casting processes, such as sand casting or high pressure die casting, can be identified.

High cooling rate in conventional casting generally leads to smaller grains in aluminum alloys, with a few rare exceptions [54][55]. In CDS, it is not so clear. Symeonidis, Shankar, and Saha et al. each showed qualitatively the effect of varied cooling rate in CDS of Al-4.5%Cu, which is detailed in Figure 12 [26][36][56]. Evidently, increased cooling rate led to the breakdown of globular morphology into a rosette-like shape. This would indicate that a slower cooling rate is favorable, meaning a casting process like sand casting may be ideal. These cooling rate ranges, however, do not encompass the full range of cooling rates available to common casting processes such as HPDC or even permanent gravity molds. Furthermore, other SSM processes are known to have severe fluidity issues, making them only suitable to HPDC. Birsan and Ashtari worked to identify conditions and alloys suitable for tilt pour gravity casting in a permanent mold, but did not explore the effects of cooling rate [57][48][49]. A higher cooling rate more representative of likely casting methods for CDS should be explored.

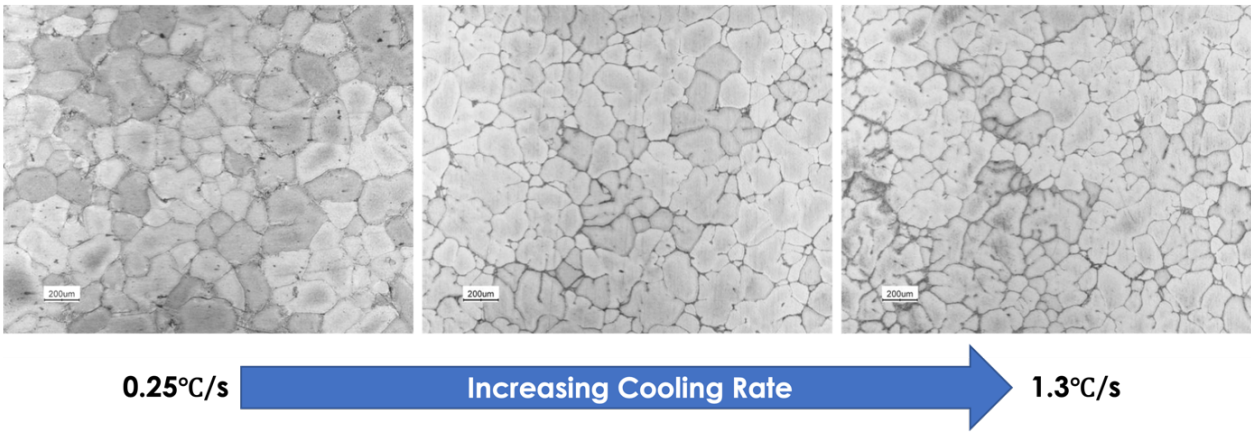


Figure 12: Effect of cooling rate on microstructures produced by CDS [35].

Symeonidis et al. explored the effect that a superheat in the pure Al HTM would have qualitatively on the microstructure of Al-4.5%Cu by CDS [35]. The results are shown in Figure 13. They found that the higher the superheat, the "less globular" the microstructure became. It is important then, at least in Al-4.5%Cu, that the pure Al HTM should be fixed at a relatively low superheat. It also introduces another intriguing parameter, the difference in temperature between precursors, ΔT_p.

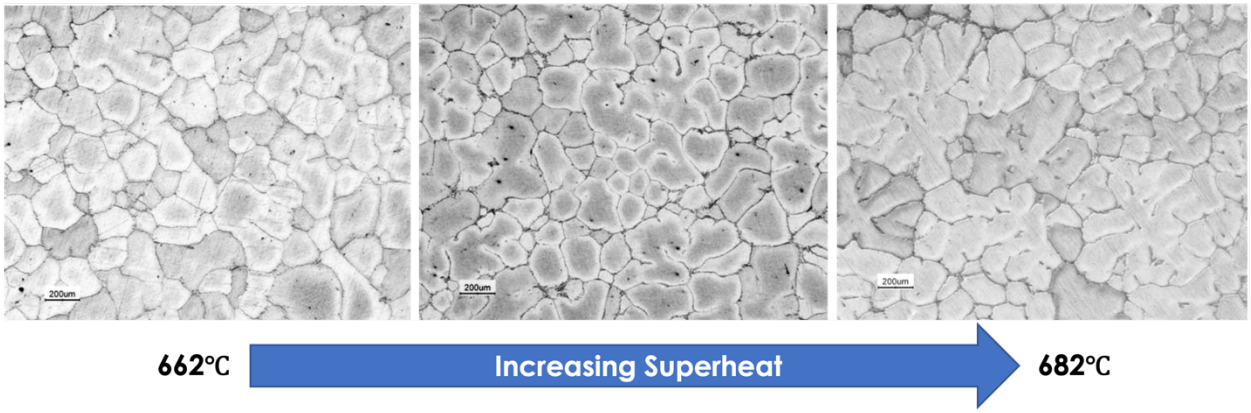


Figure 13: Effect of superheating the HTM on microstructures produced by CDS [35].

CDS experiments so far have been conducted with the temperature of both liquids within a few degrees of their respective liquidus, as shown in Table 25. The exceptions being the superheat experiment detailed above and a single experiment by Ghiaasiaan [51]. Ashtari et al.

proposed that ΔT_p should be at least 80°C and should be entirely dependent upon the liquidus of the precursor alloys [57]. With the temperature of each alloy fixed to its liquidus, ΔT_p can be considered entirely dependent on final composition and mass ratio. The effect of varying the HTM temperature has been observed, but not of varying the temperature of the LTM. Furthermore, chemical and thermal equilibration occur simultaneously at the onset of mixing in CDS. To remove chemical equilibration is simply to cast a conventionally homogenous melt. To remove thermal diffusivity, the best method is to set ΔT_p equal to 0, which is to say HTM and LTM are the same temperature. This work will observe the effect of varying ΔT_p by varying the temperature of the LTM from ΔT_p=0°C to a temperature below its liquidus, where solid should already exist.

Khalaf et al. and Chen et al. have studied the effect that mixing rate has on castings produced by CDS [2][41]. Khalaf et al. used a mixing technique representing nearly all CDS experimental procedure, wherein the HTM is poured into the LTM. Chen et al. used a technique unique to their study, shown in Figure 14, in which the HTM and LTM were poured simultaneously into a preheated crucible to mix. First contact between the two precursors occurred before they landed in the crucible. They each found that a higher mixing efficiency resulted in a more refined microstructure with a more globular shape, which can be seen in Figure 15.

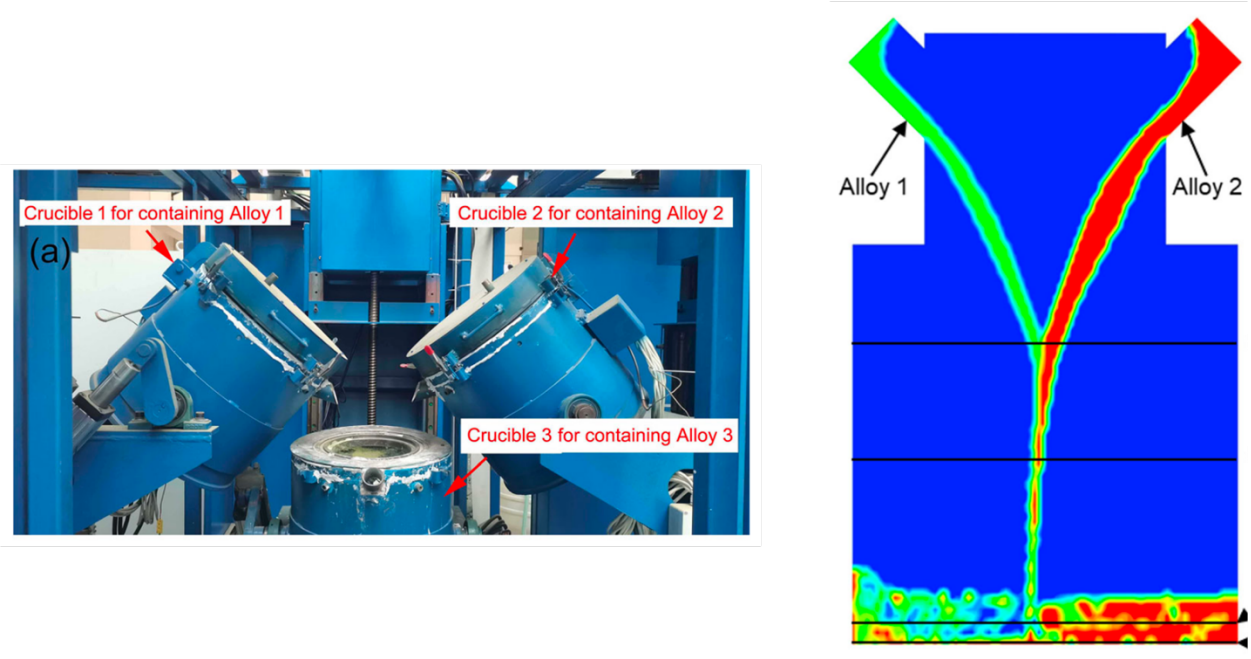


Figure 14: Simultaneous mixing apparatus for CDS [2].

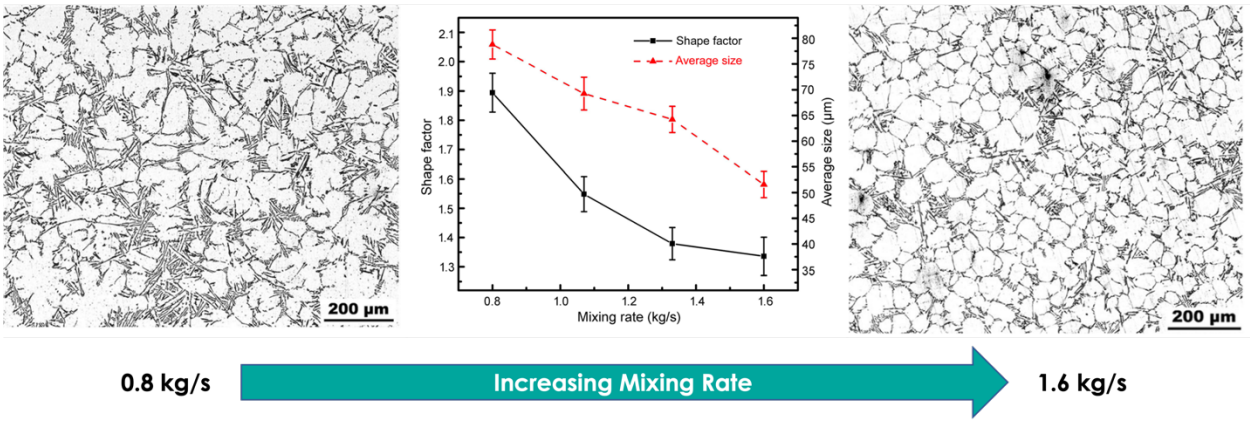


Figure 15: Simultaneous mixing [2].

Ultimately, the experiments performed thus far have been at a small scale. The largest casting with geometry by CDS was approximately 900g [1], while the largest overall was 4kg by simultaneous pouring [2]. To scale the process up for industrial use, it is necessary to better understand the effects of more process parameters on the morphology and severity of hot tearing. Further, while it is assumed that a smaller, more globular microstructure is preferable to reduce

hot tearing based on the convention of other methods of casting wrought aluminum alloys, the purported mechanisms in CDS are not the same as those methods and may therefore not reduce hot tearing via the same conventions. It is imperative, then, to clarify whether the globular microstructure is achieved via grain density, as with other SSMs, or by its own unique route as is suggested in literature. Hot tearing behavior in CDS must also be observed to confirm its ability to limit hot tearing in wrought alloys. In addition to hot tearing, flowability is a major obstacle in casting certain aluminum alloys. Many casting alloys incorporate significant amounts of Si to make it easier to fill a mold. The high latent heat of fusion of the silicon phase of Al-Si eutectic inhibits the solidification of the alloy enough that it does not solidify prior to a full fill of the mold. A high superheat can make filling easier as well but has tradeoffs. CDS is designed to cast wrought alloys, most of which have low Si content. Further, CDS is operated with fixed temperatures with little to no superheat. As with other SSMs, CDS may not be suitable for all casting processes, and it will be important to identify for which of those processes it is.

Chapter 3: Materials and Experimental Methods

3.1 Materials

Precursor alloys and homogenous conventional melts were produced with the use of 99.8% pure Al ingots and a series of master alloys presented in Table 2. Thermo-Calc software was used to design compositions of precursors based on mass ratio and liquidus temperature. Table 3 shows the targeted precursor compositions. Conv. denotes a conventional homogenous melt. HTM and LTM are precursors for CDS experiments. The high thermal mass (HTM) precursor contains the higher temperature and higher mass. It is typically pure Al or has a relatively low solute content. The low thermal mass (LTM) is held at a lower temperature and has a lower mass. It typically contains a majority of the solute present in the final composition.

Table 2: Master alloys used to create precursor alloy compositions.

Element	Master Alloy
-	99.8%Al
Cu	Al-57%Cu
Si	Al-50%Si
Mg	Al-50%Mg
Cr	Al-20%Cr

Table 3: Precursor alloys used in casting experiments.

Alloy	Al	Cu	Mg	Si	Cr
Target Compositions					
Al-Cu Conv.	balance	4.5%	-	-	-
6061 Conv.	balance	0.3%	1%	0.6%	0.2%
Al-Cu HTM	99.8%	-	-	-	-
Al-Cu LTM 1	balance	33%	-	-	-
Al-Cu LTM 2	balance	22.5%	-	-	-
6061 HTM	balance	-	-	-	0.2%
6061 LTM	balance	1.8%	6%	3.60%	-
Measured Compositions					
6061 HTM	balance	-	-	-	0.213
6061 LTM	balance	1.69	5.74	3.37	-

The Al-Cu precursor alloys were produced in small batches for direct use in experiments. Both 6061 precursor alloys were produced in large batches in an induction furnace and degassed before being poured into ingots. All castings and alloys were chemically analyzed using a SPECTROLAB S spark optical emissions spectrometer (OES). Measured compositions are displayed in Tables 3 and 4 for the 6061 precursors. Final compositions for the Al-Cu experiments will be listed in the results section. Relative standard deviation (RSD) is a mean normalized standard deviation calculated by:

(3)

in which s is the standard deviation and $\underline{x}$ is the mean.

3.2 Experimental Methods

3.2.1 Melting and Casting

The largest castings produced in the course of experiments weighed 1.2 lbs., and most weighed less than 0.5 lbs. Further, many of the experiments required mixing of two unique precursors at separate temperatures, which will be detailed later. For this reason, two Type 30400 Thermolyne box furnaces, shown in Figure 16, were used to melt all alloys to be used for experiments. Alloys were placed in No. 1 clay graphite crucibles for melts less than 0.9 lbs. or No. 4 clay graphite crucibles shown in Figure 16 for larger melts. The crucibles were coated in Boron Nitride and baked at 110 °C to dry prior to melting.

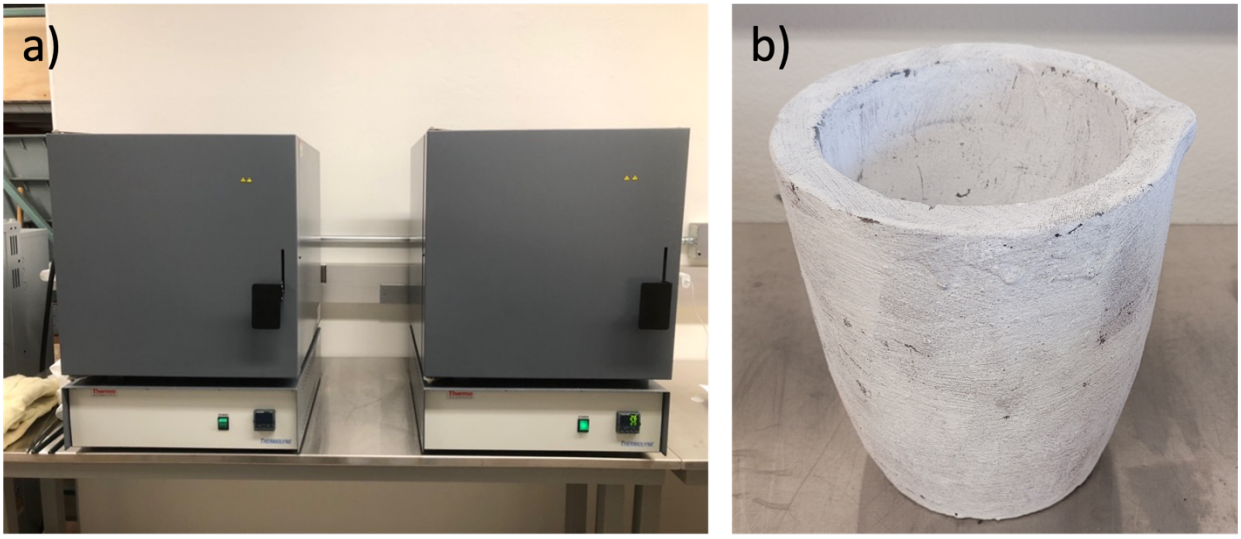


Figure 16: (a) Box furnaces and (b) graphite crucibles used for melting.

Conventional alloys were melted in box furnaces at 690°C in graphite crucibles. Approximately 20 minutes before pouring, the melts were stirred to disturb sedimentation. Once ready to pour, each melt was removed from the furnace and set on a heat resistant surface. A K-type thermocouple was used to remove oxide layers at the top of the melt and measure its temperature. Once the melt reached a superheat of approximately 10°C, it was poured into a mold designated in Tables 5-11.

The total mass of the final composition is ~200g for all experiments, except the hot tearing tests, the table for which indicates includes the mass. Precursor 1 is the high thermal mass (HTM) precursor alloy. Precursor two is the low thermal mass (LTM) precursor alloy. The mass ratio listed is the mass ratio of HTM to LTM, with the relative mass of the HTM being the larger number. P1 T is the temperature at which the HTM is poured, and P2 T is the temperature of the LTM at the same moment. T_L P1 is the liquidus temperature of the HTM, and T_L P1 is the liquidus of the LTM. Details of each experiment will use the framework in Figure 17 as a reference.

Precursor alloys used for CDS were melted in separate box furnaces based on liquidus temperature. HTMs, were melted and held in graphite crucibles at 670°C, just 10°C above liquidus. LTMs, were melted and held in graphite crucibles at 690°C, well above liquidus, to allow plenty of time to prepare to pour.

Once CDS precursors were liquid, each was stirred approximately 20 minutes before mixing. The mold for each run was placed on a heat resistant surface to await casting. The LTM was removed first from the furnace and placed on the heat resistant surface. A K-type thermocouple was used to remove oxide layers at the top of the melt and measure its temperature. Once the melt reached a superheat of approximately 15°C, the HTM was removed from the other furnace. The oxide layer on the HTM was quickly removed, temperature of the HTM was checked, in some cases the thermocouple was replaced in the LTM to log thermal data, and the HTM was poured with significant mass flow into the LTM. This will be considered the mixing step in CDS, hereafter. Immediately following the mixing step, the now mixed liquid was poured into the mold of choice. The process necessitated two people, but three were often used. The framework of the CDS experiments can be found in Figure 17.

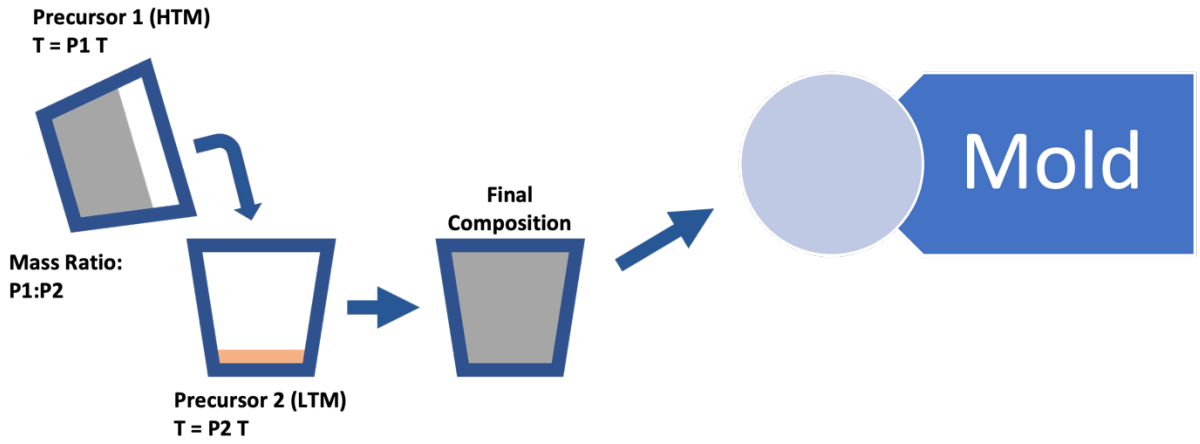


Figure 17: Framework for all CDS experiments.

3.2.1.1 Cooling Rate

An experiment in which cooling rate was varied for both CDS and for both conventionally cast and CDS cast Al-4.5%Cu. Two cooling rates, 0.2°C/s and 12.8°C/s were used. The details are listed in Table 4.

Table 4: Varying the cooling rate of Al-4.5%Cu castings.

Precursor 1 (HTM) Comp.	Precursor 2 (LTM) Comp.	Mass Ratio	P1 T (°C)	P2 T (°C)	T_L P1 (°C)	T_L P2 (°C)	Cooling Rate (°C/s)
Al	Al-33%Cu	6.33	665	553	660	548	12.8
Al	Al-33%Cu	6.33	665	553	660	548	0.2
Al-4.5%Cu Conventional Homogenous Melt							12.8
Al-4.5%Cu Conventional Homogenous Melt							0.2

Pure Al was the HTM, which was poured into an AL-33%Cu LTM. To achieve Al-4.5%Cu, the mass ratio was 6.33g of HTM to every 1g of LTM.

The same experiment was repeated in 6061 shown in Table 5.

Table 5: Varying the cooling rate of 6061 castings.

Precursor 1 (HTM) Comp.	Precursor 2 (LTM) Comp.	Mass Ratio of 1:2	P1 T (°C)	P2 T (°C)	T_L P1 (°C)	T_L P2 (°C)	Cooling Rate (°C/s)
Al-.2%Cr	Al-6Mg-3.6Si-1.8Cu	5	665	610	660	605.5	12.8
Al-.2%Cr	Al-6Mg-3.6Si-1.8Cu	5	665	610	660	605.5	0.2
6061 Conventional Homogenous Melt							12.8
6061 Conventional Homogenous Melt							0.2

Al-0.2%Cr was the HTM, and Al-6%Mg-3.6%Si-1.8%Cu was the LTM. The mass ratio was 5:1 and resulted in a nominal 6061 composition.

3.2.1.2 Thermal Data

Thermal curves were obtained during the mixing step of CDS for both Al-4.5%Cu and 6061. Table 6 details the parameters used for each alloy.

Table 6: Parameters used to obtain thermal curves during the mixing step of CDS.

Precursor 1 (HTM) Comp.	Precursor 2 (LTM) Composition	Mass Ratio	P1 T (°C)	P2 T (°C)	Equilibrium T (°C)	T_L Mixed Comp. (°C)	Mold Type
Al	Al-33%Cu	6.33	665	553	649.7	648.4	Graphite
Al-.2%Cr	Al-6Mg-3.6Si-1.8Cu	5	665	610	655.8	652.6	Graphite

Equilibrium temperature is the temperature that the mixed precursors should be based on rule of mixtures. T_L Mixed is the liquidus temperature of the final composition.

Precursor 1 (HTM) Comp.	Precursor 2 (LTM) Comp.	Mass Ratio of 1:2	P1 T (°C)	P2 T (°C)	T_L P1 (°C)	T_L P2 (°C)	Cooling Rate (°C/s)
Al-.2%Cr	Al-6Mg-3.6Si-1.8Cu	5	665	610	660	605.5	12.8
Al-.2%Cr	Al-6Mg-3.6Si-1.8Cu	5	665	610	660	605.5	0.2
6061 Conventional Homogenous Melt							12.8
6061 Conventional Homogenous Melt							0.2

3.2.1.3 Effect of Varying T between Precursors (ΔT_P)

A study of the effect of the difference in temperature between HTM and LTM was conducted. Table 7 shows the parameters used for Al-4.5%Cu, and Table 8 shows the parameters for 6061.

Table 7: Al-4.5%Cu parameters varying the temperature between precursor alloys (ΔT_P).

Precursor 1 (HTM) Comp.	Precursor 2 (LTM) Comp.	Mass Ratio of P1:P2	P1 T (°C)	P2 T (°C)	ΔT_P (°C)	T_L P1 (°C)	T_L P2 (°C)	P2 F_S	Mold Type
Al	Al-22.5%	4	665	665	0	660	594	0	Graphite
Al	Al-22.5%	4	665	599	66	660	594	0	Graphite
Al	Al-22.5%	4	665	585	80	660	594	15	Graphite
Al	Al-22.5%	4	665	570	95	660	594	25	Graphite

Al	Al-22.5%	4	665	599	66	660	594	0	Graphite
Al	Al-22.5%	4	665	585	80	660	594	15	Graphite
Al	Al-22.5%	4	665	570	95	660	594	25	Graphite

Table 8: 6061 parameters varying the temperature between precursor alloys (ΔT_P).

Precursor 1 (HTM) Comp.	Precursor 2 (LTM) Comp.	Mass Ratio of P1:P2	P1 T (°C)	P2 T (°C)	ΔT_P (°C)	T_L P1 (°C)	T_L P2 (°C)	P2 F_S	Mold Type
Al	Al-6Mg-3.6Si-1.8Cu	5	665	665	0	660	605.5	0	Graphite
Al-.2%Cr	Al-6Mg-3.6Si-1.8Cu	5	665	665	0	660	605.5	0	Graphite
Al-.2%Cr	Al-6Mg-3.6Si-1.8Cu	5	665	610	55	660	605.5	0	Graphite
Al-.2%Cr	Al-6Mg-3.6Si-1.8Cu	5	665	594	71	660	605.5	0.2	Graphite

3.2.1.4 Effect of Mass Ratio and Mixing

Table 9 shows the casting parameters used to study the effects of varying mass ratio and mixing in CDS of Al-4.5%Cu.

Table 9: Al-4.5%Cu experimental parameters varying the mass ratio between precursor alloys.

Precursor 1 (HTM) Comp.	Precursor 2 (LTM) Comp.	Mass Ratio of P1:P2	P1 T (°C)	P2 T (°C)	ΔT_P (°C)	T_L P1 (°C)	T_L P2 (°C)	Resultant T (°C)	Mold Type
Al	Al-33%Cu	6.33	665	553	112	660	548	650	Graphite
Al	Al-22.5%	4	665	599	66	660	594	652	Graphite

3.2.1.5 Hot Tearing

Table 10 shows the casting parameters used to test the susceptibility of 6061 cast by CDS to hot tearing.

Table 10: 6061 experimental parameters testing hot tearing susceptibility.

Precursor 1 (HTM) Comp.	Precursor 2 Comp.	Mass Ratio of P1:P2	P1 T (°C)	P2 T (°C)	T_L P1 (°C)	T_L P2 (°C)	Mold Type	Mass Final Comp.
Al-.2%Cr	Al-6Mg-3.6Si-1.8Cu	5	665	610	660	605.5	Sand	680g
Al-.2%Cr	Al-6Mg-3.6Si-1.8Cu	5	665	610	660	605.5	Permanent	400g
6061 Conventional Homogenous Melt							Sand	680g
6061 Conventional Homogenous Melt							Permanent	400g

3.2.2 Mold Design and Procedure

Four types of molds were used for both conventional and CDS experiments. The molds are listed in Tables 4-10. Graphite and steel molds were used to observe microstructure under varied cooling regimes. Cooling rates for each were calculated from cooling curves obtained during castings. Hot tearing molds were designed and built with sand to test susceptibility to hot tearing. The tensile bar mold was a permanent H13 tool steel mold used to further test hot tearing with a faster cooling rate than the sand molds. Each is described with more detail below.

The graphite molds were the same clay graphite No. 1 molds, shown in Figure 18, used for melting. The molds were preheated to 690°C before being placed on the heat resistant surface. Melts were poured directly into the crucibles and let solidify completely before moving. Castings were not removed from the graphite crucible until they were completely cool. Castings made this way are about two inches in diameter and one inch in height, as shown in Figure 18.

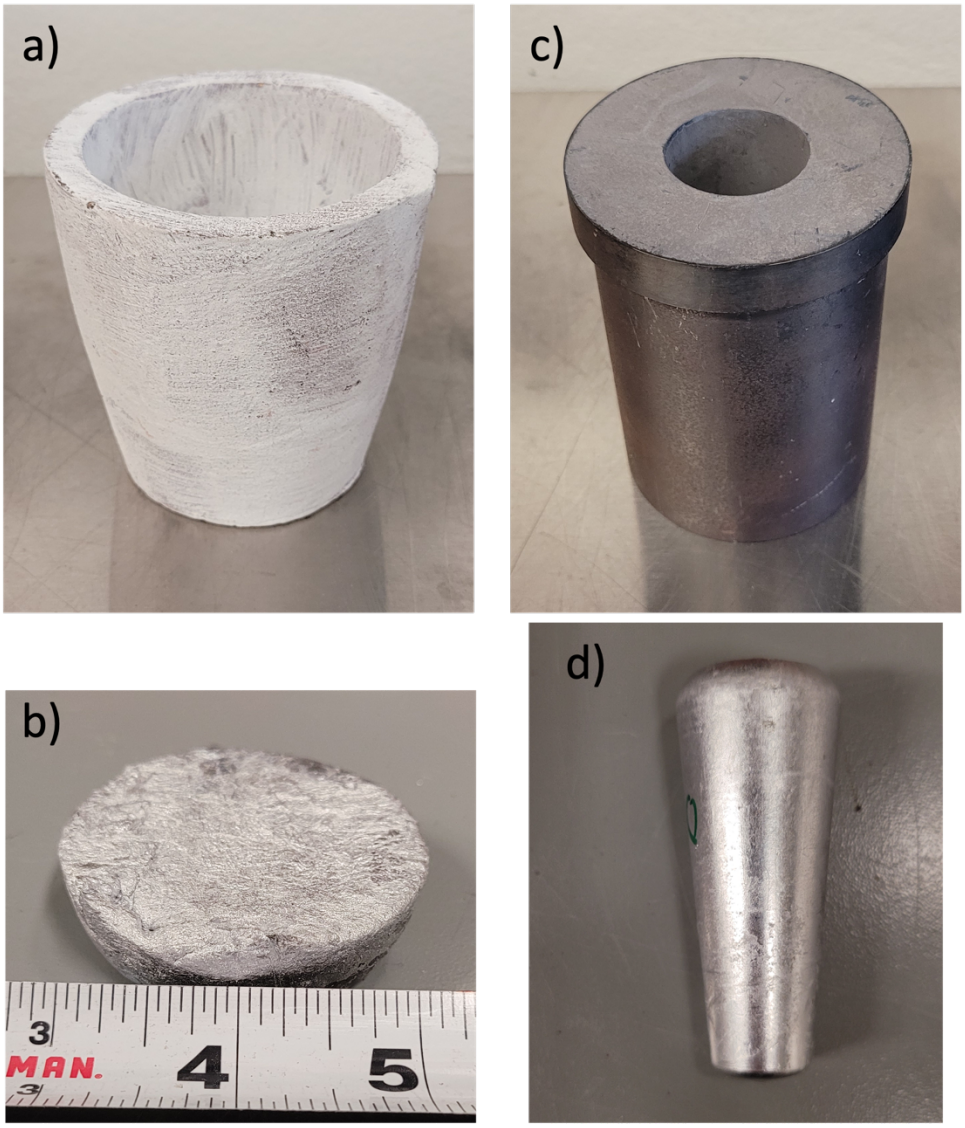


Figure 18: (a-b) Graphite mold and casting produced from it and (c-d) steel mold and casting produced from it.

The steel mold, shown in Figure 18, was preheated to 350°C before being placed on the heat resistant surface. Melts were poured directly into the mold and let solidify completely before being removed. As soon as the castings were completely solidified, they were removed from the steel mold to air cool. Castings poured into the steel mold, and, therefore, the cavity of the mold, had a smaller diameter of 3/4 of an inch, a larger diameter of 1 1/8 inch, and a height of 2.5 inches.

Sand molds meant to test the hot tearing susceptibility of alloys were designed by Dr. Carl Söderhjelm based on an N-Tec hot tearing mold described by Akhyar et al. and Li and Apelian [2][58]. Simulations were performed in Magmasoft to ensure full fill would be achieved. The sand molds are depicted in Figure 19. Protrusions at the end of the arms are meant to keep them stationary and apply longitudinal stress to the arms as they solidify and shrink. Longer arms should experience more stress as shrinkage strain is applied over a longer distance. A negative for the mold, shown in Figure 19d, and another for the sprue were additively manufactured based on the schematic in Figure 19e, and sand with an activated, water-soluble binder was packed around the negatives. The packed sand was left to bind for at least an hour before the negatives were removed., after which the molds were left to cure completely overnight. Prior to casting, the molds were placed on a heat resistant surface and the sprue placed on top.

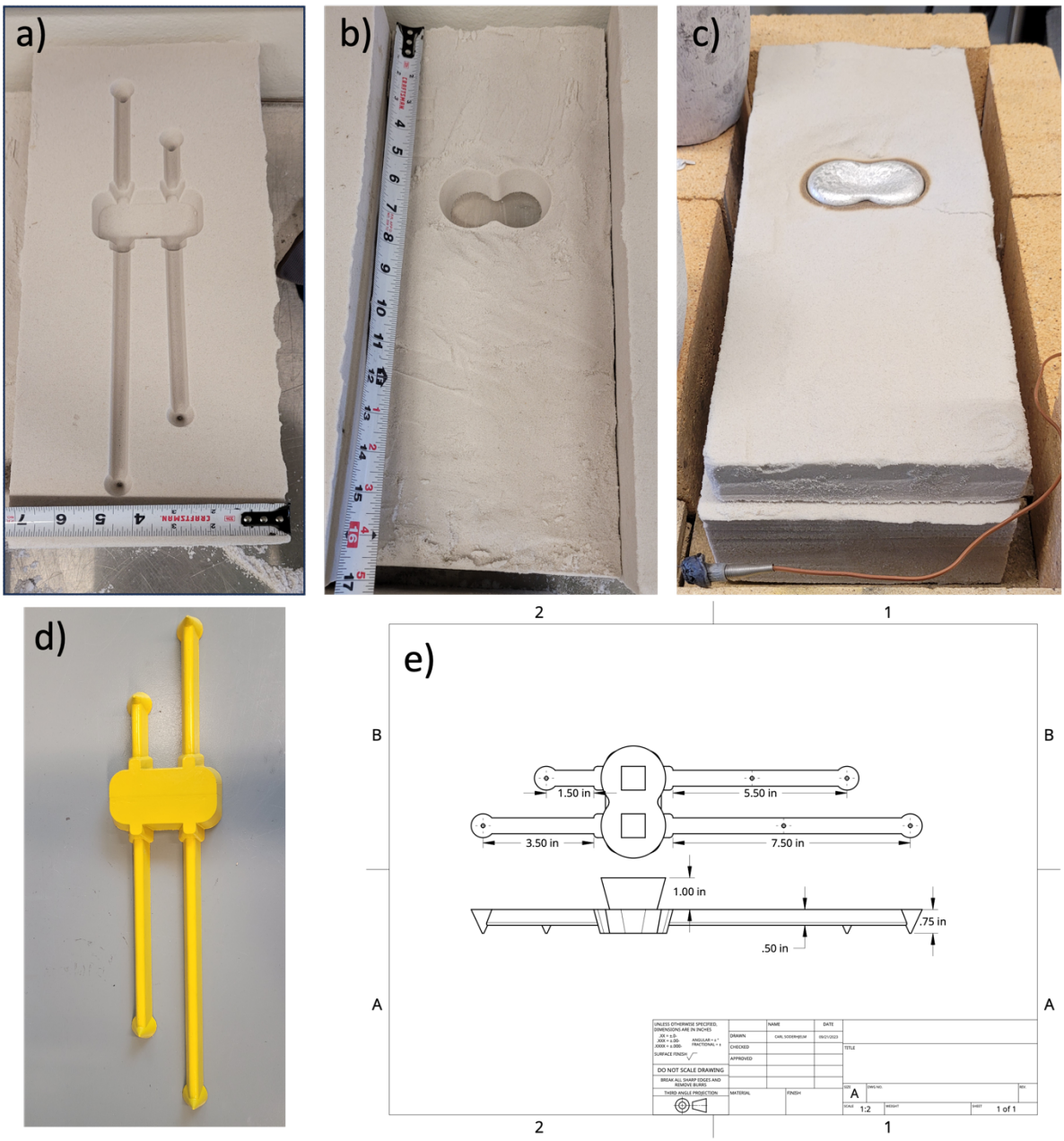


Figure 19: (a) Hot tearing sand mold, (b) sprue piece, and (c) both mold and sprue in action.

The tensile bar mold meeting the specification listed in ASTM B108 is a permanent steel mold meeting the specification listed in ASTM B108 [58]. Figure 20 shows the mold with a part of a previous casting inserted. The partial casting was preheated to 110°C to remove any moisture and placed into the mold to block those parts of the mold. This would allow small scale

castings of tensile bars while minimizing the danger of partial fill due to any fluidity issues related to CDS as an SSM. If the sand mold hot tearing was meant to test at low cooling rates, the tensile bar mold was meant to test hot tearing at increased cooling rates. The mold was preheated to 445°C to maximize flowability and set on a steel plate for casting.

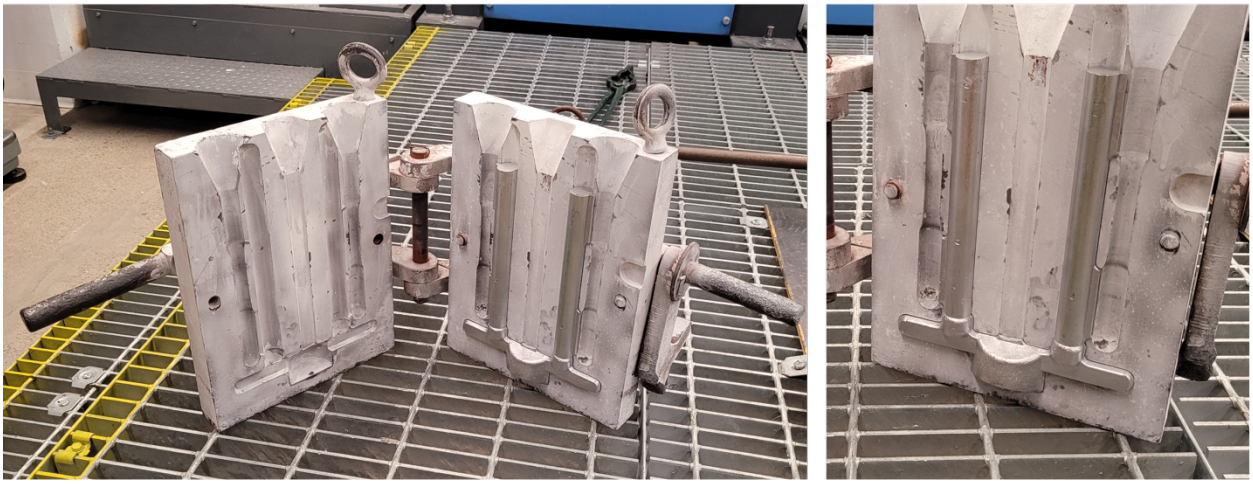


Figure 20: Tensile bar permanent mold with precast insert.

3.2.3 Materials Characterization

Sections were taken from the same location for each sample for characterization. Figure 21 shows the location of the sections taken from castings in the graphite crucibles. Cross sections were taken from the steel mold samples 1 inch up from the smaller diameter. Sections were cut from the longest arm of three of the sand mold castings, .5 inches from the base of the arm. All samples were cut using the Buehler AbrasiveMet M.

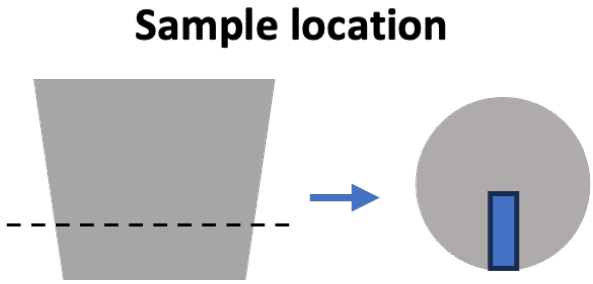


Figure 21: Location of samples taken from clay graphite mold castings.

Compositions were obtained for all samples produced in this work using the SPECTROLAB S spark OES. Samples poured into graphite crucibles were cut down the middle and the compositions were obtained consistently from five locations shown in Figure 22a. The order shown was kept consistent throughout all samples. Compositions from samples produced during hot tearing tests in the sand molds were taken from the bottom of the samples with the same configuration, shown in Figure 22b.

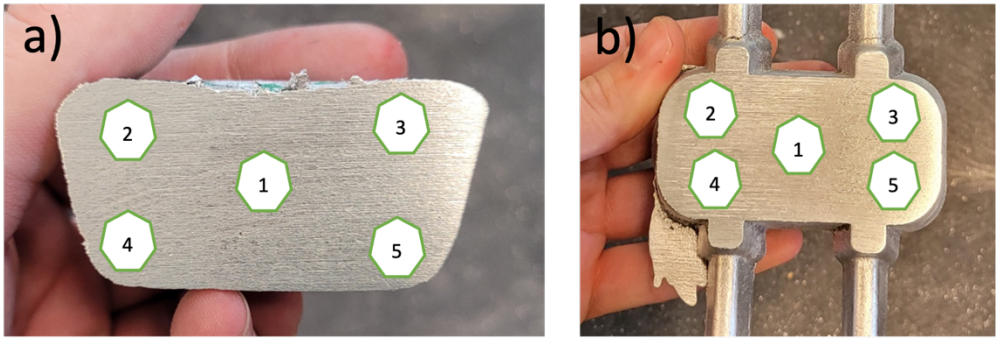


Figure 22: OES spark locations for (a) graphite cast samples and (b) sand mold samples.

All samples were mounted in KonductoMet mounting powder by the Buehler Simplimet 4000 hot mounting system. Samples were ground and polished using the Buehler AutoMet 250 and anodized in the Buehler ElectroMet 4. The anodizing electrolyte was 2% fluoroboric acid in water, otherwise known as Barker's reagent [59]. Copper tape was used to create a conductive pathway from the cathode to the face of the sample and voltage was set to 20V for 1 minute and 20 seconds.

Anodized samples were imaged under polarized light using an Evident Scientific digital microscope. The combination of anodization by Barker's and polarized light revealed the grain structure for size and morphology characterization. Images were taken under minimum zoom and with a 4x4 stitching to get a representative microstructure. Further micrographs were obtained using a Quanta3D scanning electron microscope (SEM).

Characterization of the micrographs was performed using GIMP image editing software to trace the grains in a representative area and ImageJ FIJI to obtain average grain area and circularity. Grain area was a function of pixel count per grain, but circularity was defined by

(4)

in which A and P is perimeter. Figure 23 shows a visual representation of the circularity. Circularity is calculated to quantify the effect that CDS has on the globular microstructure, and, potentially, the effect globularity has on hot tearing.

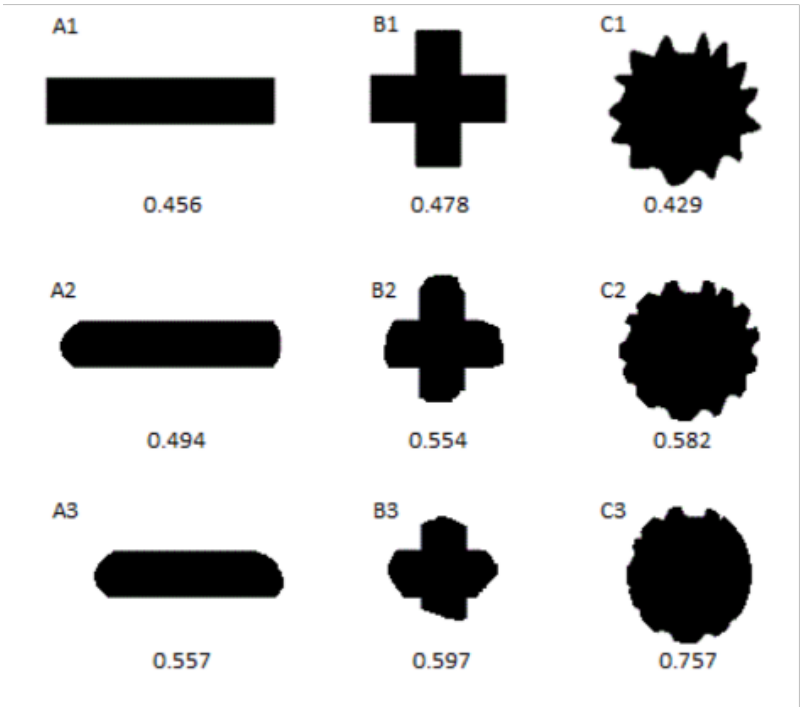


Figure 23: Visual representation of circularity [60].

Chapter 4: Results and Discussion

The goal of this work is to deepen the understanding of Controlled Diffusion Solidification and transition it from laboratory-scale experimentation to industrial application. This involves examining key parameters such as cooling rate, temperature differentials between precursors, and mass ratios, to assess their influence on the castability of wrought aluminum alloys.

To understand how these parameters affect the process, it is crucial to focus on the resulting microstructure. Smaller and more globular grains have been proven to mitigate the susceptibility of aluminum alloys to hot tearing [5]. This work uses grain area and circularity for a quantitative analysis of the microstructure.

The first three sub-sections will provide a quantitative evaluation of how the parameters affect grain area and circularity in the castings. First, results for Al-4.5%Cu will be presented, followed by 6061, and finally, the two will be compared.

The last two segments of this section will offer a qualitative assessment of the impact of these parameters on the castability of 6061 alloy, with an emphasis on hot tearing.

4.1 Effect of Cooling Rate

Figure 24 shows the effect of cooling rate on the microstructure of conventionally and CDS cast Al-4.5%Cu – note the logarithmic scale for the conventional graph. Grain size and circularity for each micrograph are displayed according to casting method in Table 11. Cooling rates were measured once for each mold type and generalized to each subsequent casting.

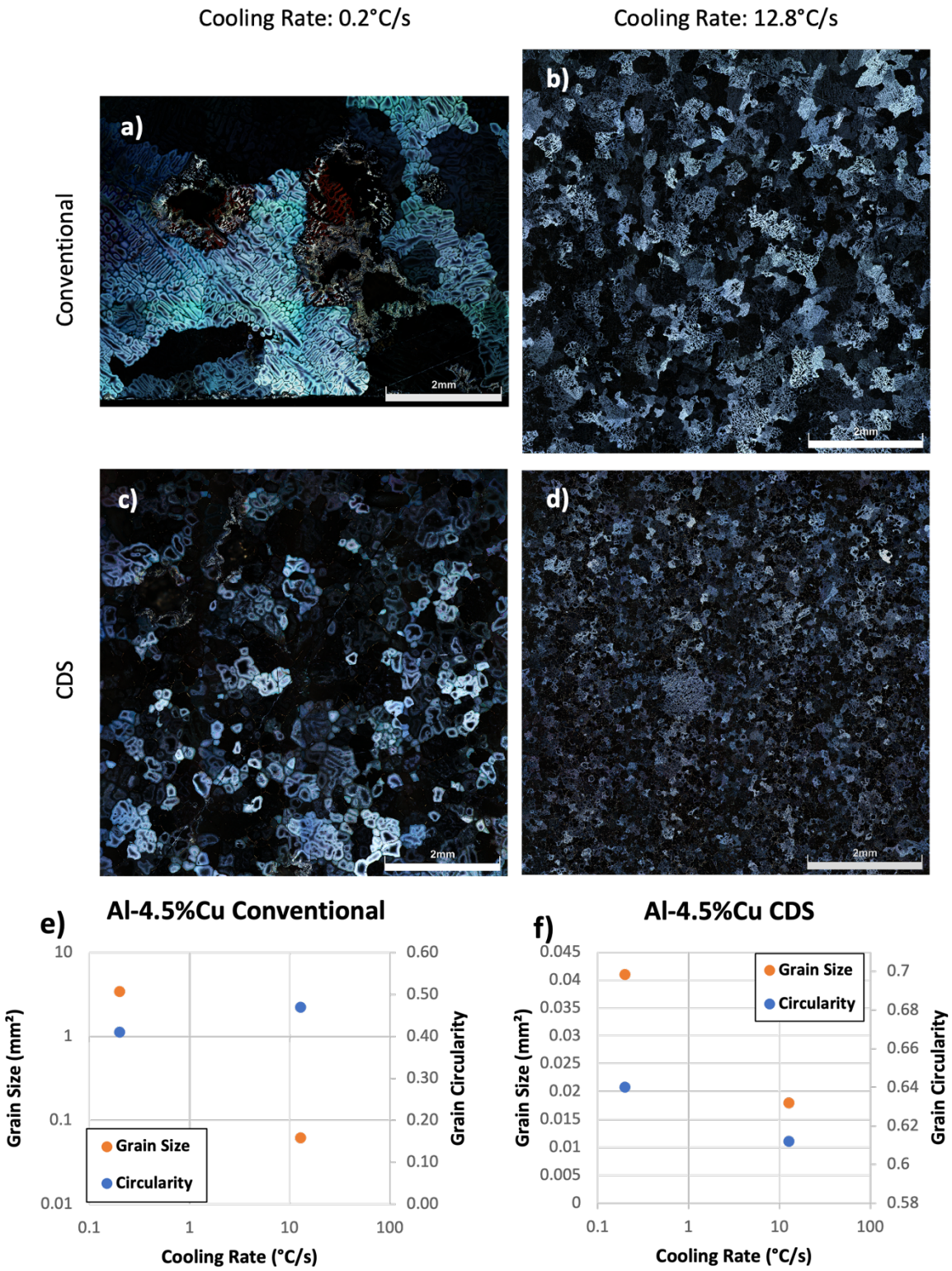


Figure 24: Anodized microstructure of Al-4.5%Cu cast by (a)-(b) conventional solidification and (c)-(d) Diffusion Solidification with cooling rates of (a)(c) 0.2 ℃/s and (b)(d) 12.8 ℃/s, and the effect of cooling rate on grain size and grain circularity in (e) conventional and (f) Diffusion Solidification castings.

Table 11: Tabulated effects of cooling rate on grain size and circularity in Al-4.5%Cu cast conventionally and by CDS.

Casting Process	Cooling Rate (°C/s)	Avg. Grain Size (mm²)	Grain Circularity
Conventional Al-4.5%Cu	0.2	3.43	0.41
Conventional Al-4.5%Cu	12.8	0.062	0.47
CDS Al-4.5%Cu	0.2	0.041	0.64
CDS Al-4.5%Cu	12.8	0.018	0.61

The effect of cooling rate on conventionally cast Al-4.5%Cu is shown in Figure 24a and Figure 24b. Higher cooling rate leads to refined grains with more circularity. This is consistent with literature which suggests that increased cooling rate is an effective method of grain refinement in Al-Cu alloys [61].

Grain refinement is achieved with the CDS process when compared to conventional casting, regardless of cooling rate. Circularity is also increased. Figure 24c and Figure 24d show that, despite significant reduction in grain size via CDS when compared to Figure 24a and Figure 24b, respectively, the morphology of the grains is still dendritic. The microstructures are consistent with literature [62][35], however, confirming the recreation of the operating procedure. Al-4.5%Cu castings produced by CDS should show improved hot tearing tendencies compared to those produced by conventional methods, according to literature.

The effect of cooling rate on the CDS process can be observed by comparing Figure 24c and Figure 24d. A higher cooling rate leads to refined grain structure in the same way as in conventional casting. There is a slight reduction in circularity at a higher cooling rate, suggesting that the globular microstructure suffers slightly under faster cooling regimes. Symeonidis et al. and Saha et al. also qualitatively observed a decrease in the globularity of grains in the CDS process with increased cooling rate [26][35]. However, the microstructures in Figure 24 show

much less drastic reductions in circularity than suggested by literature over larger cooling rate ranges.

Previous work determined that an increase in cooling rate led to a decrease in the efficacy of CDS to create a globular microstructure in Al-4.5%Cu. The cooling rates examined ranged from 0.25°C/s to 1.3°C/s in the Symeonidis study and 2°C/s to 9°C/s in the Saha study [26][35]. There is some inconsistency between the two, namely that the microstructure resulting from the 1.3°C/s casting shows a 'less globular' microstructure than that of the 2°C/s casting from the other study. The results shown in Figure 24 show a much smaller effect of cooling rate on the circularity than previously suggested with a significant effect on grain size. Since hot tearing can be reduced by *both* grain size reduction and a globular microstructure, a slow cooling rate may not be as optimal for CDS as previously thought.

Figure 24 shows the efficacy of CDS to refine grains and increase their circularity. Microsegregation revealed by the anodization shows that the grains are still dendritic in nature, despite their relatively high circularity. This is most likely a result of copious equiaxed grains limited in growth by the density of grains. The mechanisms proposed for CDS thus far suggest that globular grains form due to the subversion of dendritic growth by convective forces or a reversal of solute concentrations in front of the solid liquid interface (S/L). They do not allow for circular grains with microsegregation consistent with dendritic arms. Figure 24 shows that dendritic growth is occurring, even within the highly circular, 'globular', grains. The mechanisms for globular growth proposed thus far in literature do not allow for dendritic growth at all, so the existence of dendritic features within a circular grain is inconsistent with current understandings.

Figure 25 shows effect of cooling rate on 6061 cast conventionally and by CDS – note the logarithmic scale on the grain size axis for conventional solidification. Table 12 shows the tabulated data obtained from the microstructures. Grain size and circularity for each micrograph are displayed according to casting method. The experiment follows the same operating procedure as in Figure 24, with different parameters and compositions which are listed in the Table 4.

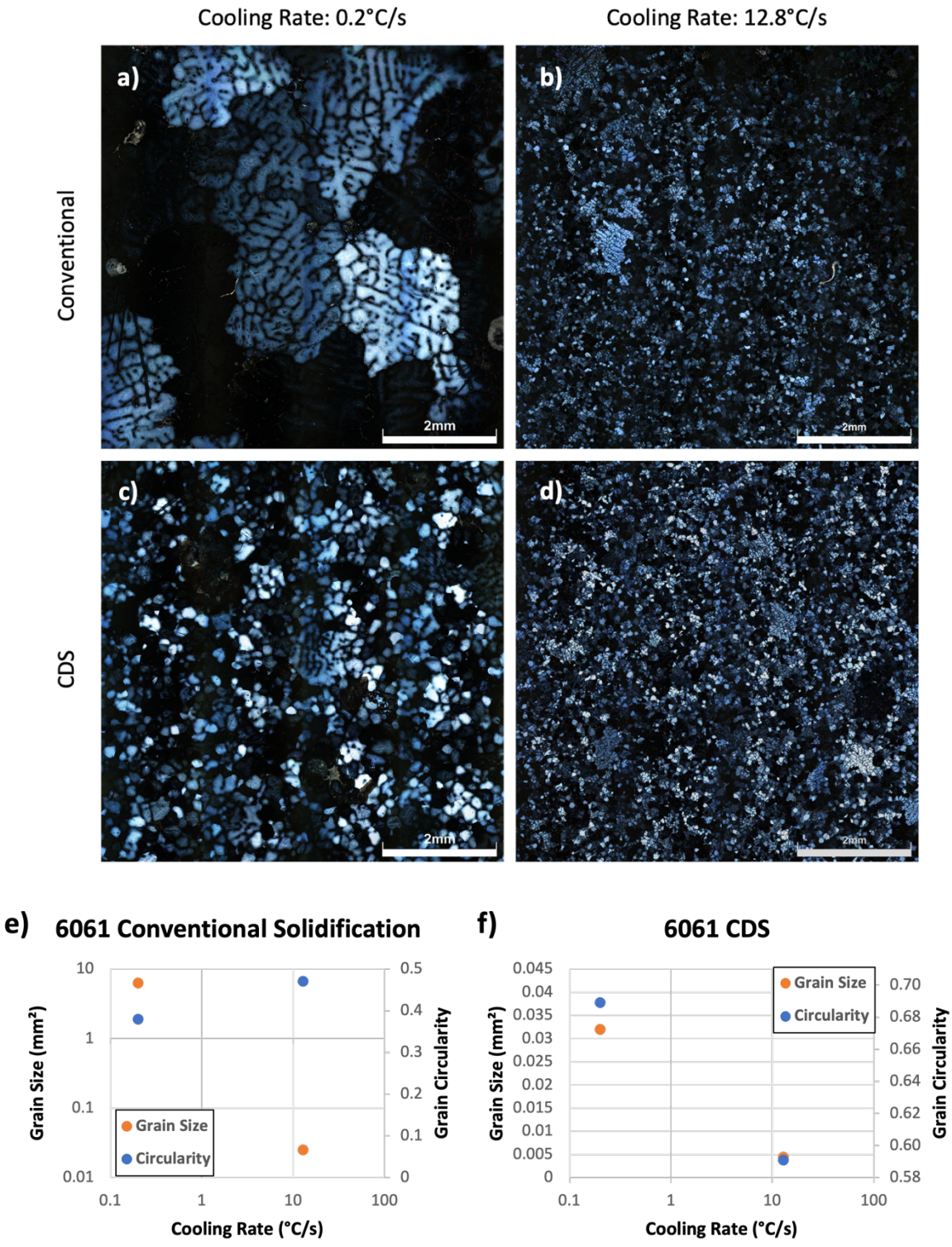


Figure 25: Anodized microstructure of AA6061 cast by (a)-(b) conventional solidification and (c)-(d) Diffusion Solidification with cooling rates of (a)(c) 0.2 °C/s and (b)(d) 12.8 °C/s, and the effect of cooling rate on grain size and grain circularity in (e) conventional and (f) Diffusion Solidification castings.

Table 12: Tabulated effects of cooling rate on grain size and circularity in 6061 cast conventionally and by CDS.

Casting Process	Cooling Rate (°C/s)	Avg. Grain Size (mm^2)	Grain Circularity
Conventional 6061	0.2	6.31	0.38
Conventional 6061	12.8	0.025	0.47
CDS 6061	0.2	0.027	0.64
CDS 6061	12.8	0.0044	0.59

CDS again shows a reduction in grain size and an increase in circularity compared to conventional casting, regardless of cooling rate. Comparing Figure 25b and Figure 25c, CDS alone appears to have similar grain refining capabilities to an increased cooling rate alone but with better resultant circularity. The biggest swing in morphology is between CDS and conventionally cast samples cooled at 0.2°C/s, suggesting diminishing returns in grain refinement when combining both increased cooling rate and CDS. Either way, the efficacy of CDS as a grain refinement method in 6061 is confirmed. The smaller grains and increased circularity should result in a reduced hot tearing tendency when comparing CDS to conventional solidification *within a particular cooling regime*.

The effect of higher cooling rate on the CDS process in 6061 is smaller grains and slightly reduced circularity. This result is consistent with the Al-4.5%Cu benchmark shown previously. Increased cooling rate has a relatively larger effect on grain size in 6061 than in Al-4.5%Cu, while also reducing circularity more. The reduction in circularity still does not seem to reach the levels reported qualitatively in literature. This suggests that there may be potential for casting 6061 by CDS in molds with high cooling rates.

Table 13 shows the effect of cooling rate on both Al-4.5%Cu and 6061, cast both conventionally and by CDS. While 6061 is more amenable to grain refinement than Al-4.5%Cu, circularity seems to be largely independent of composition and more dependent on process and

cooling rate as a function of magnitude of grain refinement. In other words, CDS and an increase in cooling rate from 0.2°C/s to 12.8°C/s have similar ability to refine grains but have different effects on circularity. When combined, the grain refining effect is compounded, resulting in smaller grains than are achievable by either method alone. The resulting circularity, on the other hand, is somewhere between – not quite as circular as attainable by CDS alone, but far better than by increased cooling rate – suggesting an average of sorts. Literature suggests that both grain size and shape play a significant role in reducing hot tearing [5], but it is unclear the relative impact each has. It is possible that the slight reduction in circularity when combining high cooling rate and CDS, compared to CDS alone, may counteract the benefits gained by further refining the grains.

A possible explanation for the effect that cooling rate has on the microstructure during the CDS process is that, assuming the possibility of solute field impingement as a mechanism for globular growth, a faster cooling rate results in a higher contribution of thermal undercooling as a driving force for solidification. It competes with curvature undercooling, solidifying the impinged solute field before curvature undercooling can smooth the dendritic features produced during unconstrained growth [12]. The natural progression as cooling rate increases, assuming near constant grain size, would be globular to rosette to equiaxed dendritic. This is represented in both Symeonidis et al. and Saha et al. studies [26][35][36]. However, cooling rate also acts as a grain refiner, somewhat counteracting the effect of the smaller DAS, although evidently not entirely. The proposed solute field impingement mechanism sufficiently explains the effect of cooling rate where other mechanisms do not.

Table 13: Effect of cooling rate on both Al-4.5%Cu and 6061.

Casting Process	Cooling Rate (°C/s)	Avg. Grain Size (mm^2)	Grain Circularity
Conventional Al-4.5%Cu	0.2	3.43	0.41
Conventional 6061	0.2	6.31	0.38
Conventional Al-4.5%Cu	12.8	0.062	0.47
Conventional 6061	12.8	0.025	0.47
CDS Al-4.5%Cu	0.2	0.041	0.64
CDS 6061	0.2	0.027	0.64
CDS Al-4.5%Cu	12.8	0.018	0.61
CDS 6061	12.8	0.0044	0.59

In summary, molds were used that exhibit cooling rates representing a wide array of casting processes, from sand casting to permanent mold. Results of the Al-4.5%Cu study are consistent with literature, confirming the recreation of the experimental procedure. Results of the 6061 study confirm that it is a suitable candidate for the CDS process, even surpassing the model Al-4.5%Cu system in refining amenability. CDS was confirmed to improve both grain size and circularity significantly over conventional casting, regardless of composition or cooling rate. Negative effects of increased cooling rate on the globularity of CDS castings were confirmed but seem to be less drastic than literature suggests. The effect of cooling rate on the microstructure can be sufficiently explained using the copious nucleation and solute field impingement mechanism proposed by Zeng et al. to explain the formation of globular grains during grain refinement using inoculants [12]. Finally, microsegregation in CDS castings suggests that the mechanisms for obtaining a globular microstructure proposed in literature thus far may not be comprehensive.

4.1.1 Thermal Data

Figure 26 shows thermal curves obtained during the mixing step of CDS of Al-4.5%Cu. The thermocouple is placed in the center of the LTM melt, in this case Al-33%Cu, and held while the HTM, pure Al, is poured into the crucible. The HTM is at a higher temperature than the LTM, resulting in a large spike in measured temperature. As soon as the two liquids meet, there should be nucleation events that release latent heat. The equilibrium temperature of the two liquids sans latent heat is approximately 650°C by rule of mixtures. The thermal curves show that the temperature rises above the equilibrium temperature, suggesting that nucleation is indeed occurring.

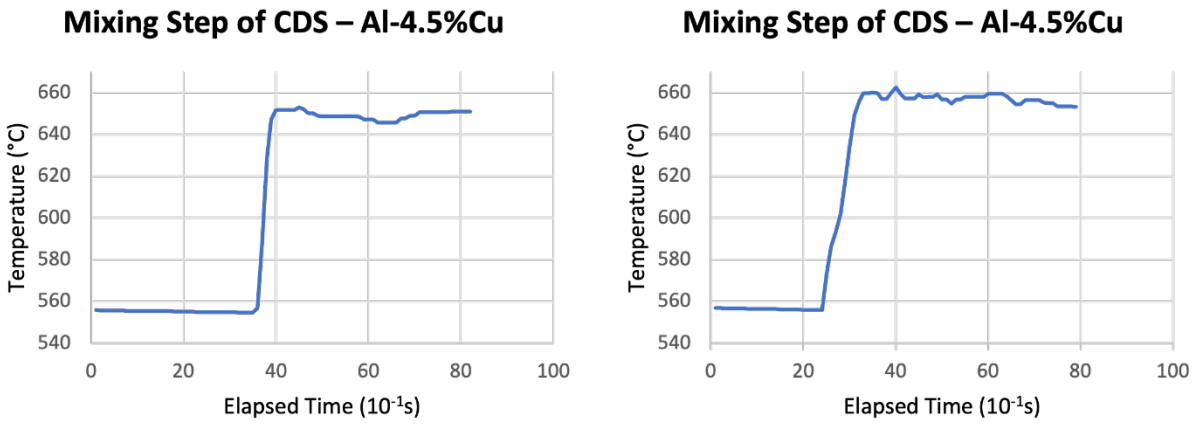


Figure 26: Thermal curves obtained during the mixing step of CDS of Al-4.5%Cu.

Figure 27 shows the same curves in 6061. The equilibrium temperature for these is 656°C. Variations in the shape and temperatures of the curves may be attributed to minute differences in mixing stemming from the location of the thermocouple. For the most part, the temperature continues to rise after temperature equilibrium occurs, again suggesting that nucleation is occurring in the first few seconds of mixing.

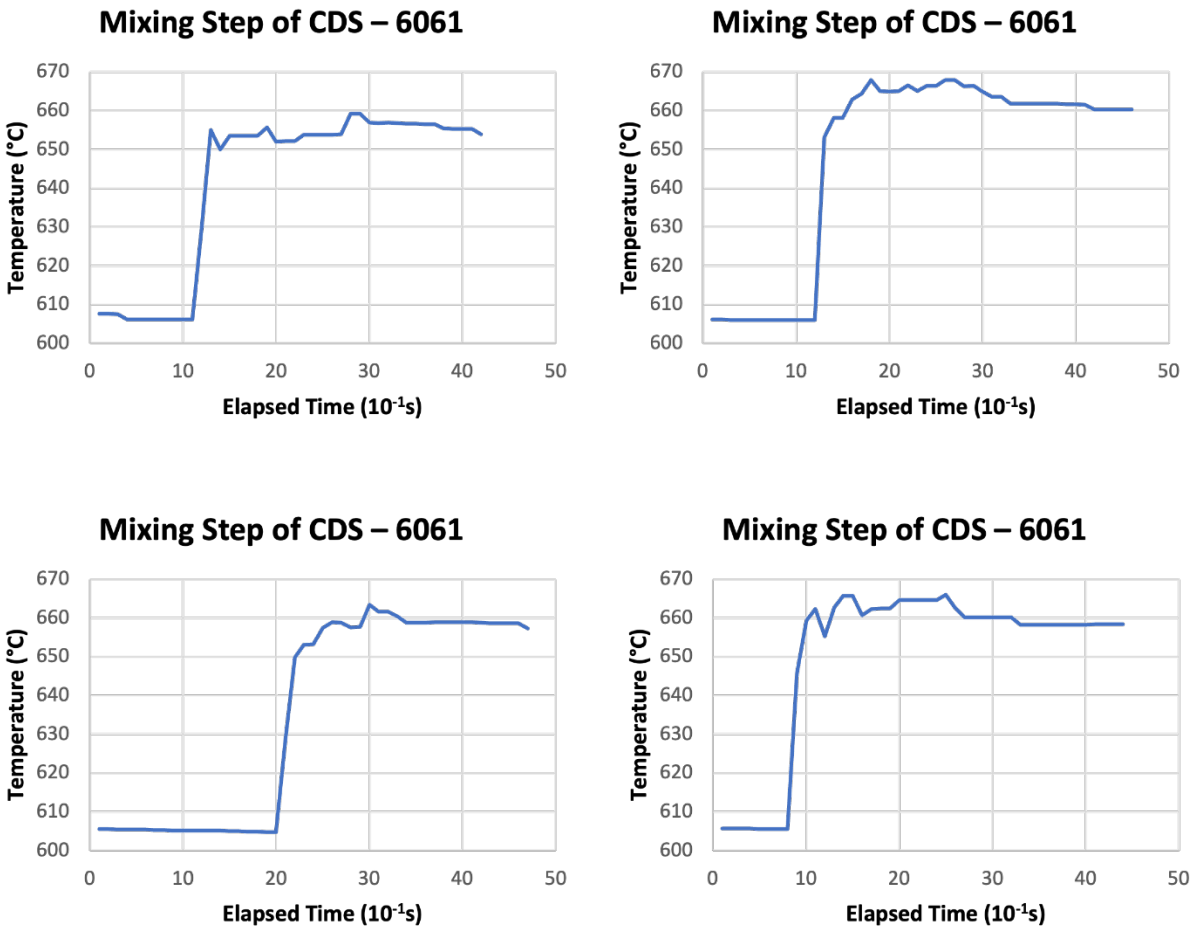


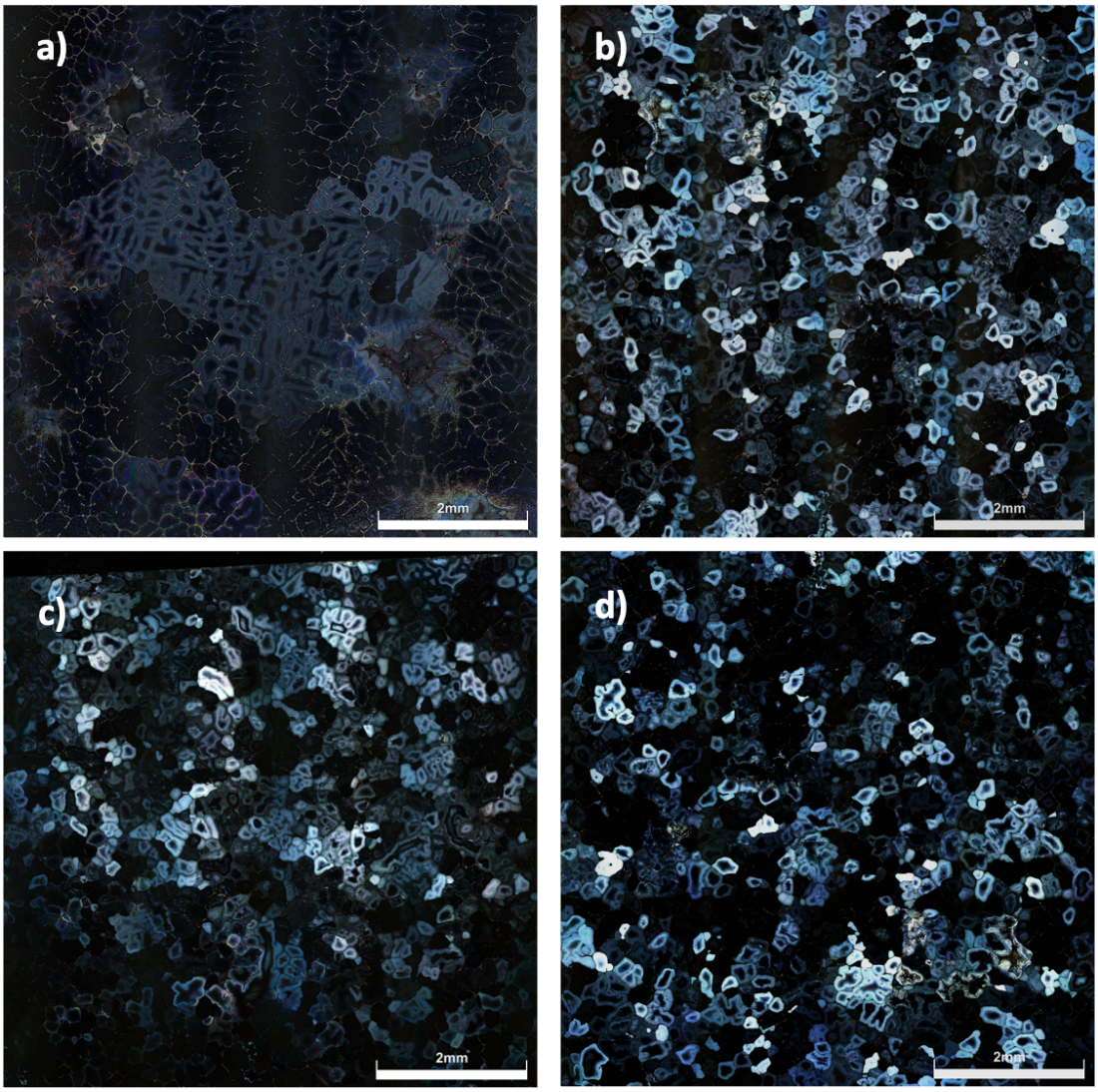
Figure 27: Thermal curves obtained during the mixing step of CDS of 6061.

4.2 Effect of Varying T between Precursor Alloys (ΔT_P)

Figure 28 shows the effect of ΔT_P on the microstructure of Al-4.5%Cu cast by CDS. Grain size and circularity for each micrograph are displayed in graph form and in tabular form in Table 14. The temperature of the HTM (Precursor 1, pure Al) was fixed to 665°C. ΔT_P was varied solely by varying the temperature at which the LTM (Precursor 2, Al-22.5%Cu), was at the onset of mixing. Al-22.5%Cu was chosen as the LTM to explore the ΔT_P space below the liquidus of the LTM, as well as to examine the effects of mass ratio on the CDS process.

Table 14: Effect of differences in ΔT_P on grain morphology in Al-4.5%Cu

ΔT_P (°C)	Precursor 2 (LTM) T (°C)	Cooling Rate (°C/s)	Avg. Grain Size (mm^2)	Grain Circularity
Conv.	-	0.2	3.43	0.41
0	665	0.2	2.14	0.33
66	599	0.2	0.048	0.59
80	585	0.2	0.044	0.65
95	570	0.2	0.035	0.52



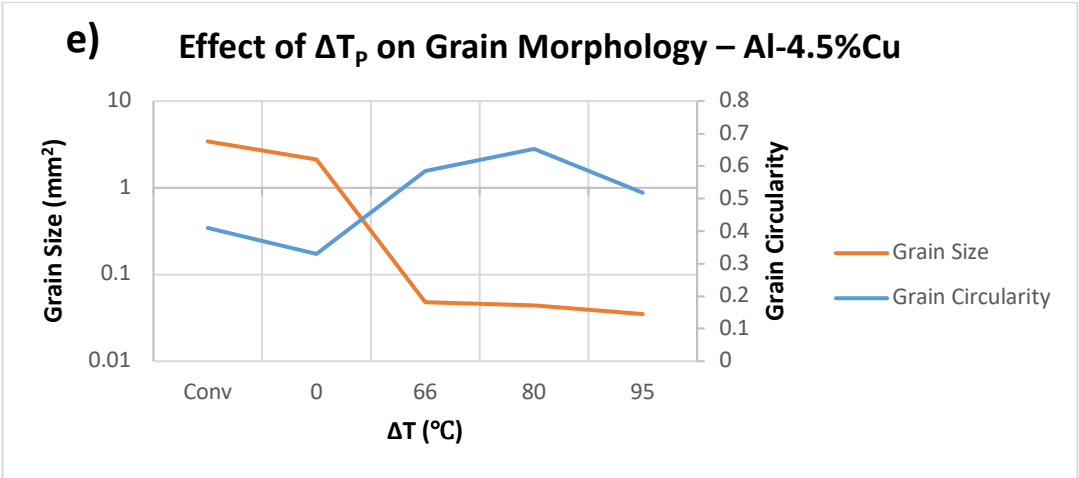


Figure 28: Anodized microstructure of Al-4.5%Cu cast by CDS with a mass ratio of 4:1 and a ΔT_P of (a) 0°C, (b) 66°C, (c) 80°C, and (d) 95°C between precursor alloys accompanied by (e) effect of the variance of ΔT_P on morphology.

When $\Delta T_P = 0°C$ in CDS, Al-4.5%Cu has large grains with low circularity resembling that of conventionally cast Al-4.5%Cu. This ΔT_P was cast to isolate chemical equilibration from thermal equilibration. It is evident that without a temperature difference causing undercooling in the pure Al HTM, copious nucleation cannot take place. It is unclear the extent to which chemical equilibration can take place.

At $\Delta T_P = 66°C$ the Al-22.5%Cu LTM is 5°C above liquidus, matching the typical recipe for CDS dictated by literature [31][57]. The grain size is not quite as refined and the circularity not as high as the previous experiment in which the LTM is Al-33%Cu and $\Delta T_P = 112°C$. This may be due to the substantial decrease in ΔT_P, which may allow for less nucleation at the onset of mixing. Ashtari et al. suggested a ΔT_P of at least 80°C for optimum results in the CDS process [57], and this result supports the claim. Further support comes from the results of the $\Delta T_P = 80°C$ casting, which matches exactly the minimum ΔT_P suggested.

At $\Delta T_P = 80°C$, the LTM is 10°C below liquidus and approximately 12 percent solid according to Scheil non-equilibrium solidification calculations performed both manually and in Thermo-Calc. Grain size is smaller than in the $\Delta T_P = 66°C$ microstructure and circularity is higher. This also supports the suggestion of a minimum of 80°C between the precursor alloys, although it suggests that the ΔT_P is not necessarily dependent upon liquidus temperatures. It should also be considered that the solid formed in the LTM prior to mixing could act as nucleation sites for rapidly undercooled pure Al HTM, forming even more nuclei and producing a higher grain density. High grain density could, in turn, account for the higher circularity. A proposed mechanism for globular grains in grain refined alloys is solute field impingement and the replacement of constitutional undercooling as the driving force for solidification by curvature undercooling [12]. Smaller grains would result in less unconstrained dendritic growth and

providing a less complex surface and allowing curvature undercooling driven solidification to smooth the dendritic features more efficiently to a more spherical – read globular – morphology.

The benefits of the increased undercooling and the possible benefits from preformed solid in the LTM are erased when $\Delta T_P = 95°C$. The LTM is 25 percent solid at 570°C, and while the average grain size trends downward still, the circularity also decreases dramatically from when $\Delta T_P = 80°C$. Most likely, enough of the solid formed in the LTM grew unconstrained, forming grains sufficient in size and with low enough circularity to skew the average circularity downward. The average grain size was reduced further by increased undercooling and potentially increased heterogeneous nucleation sites provided by the preformed solid. Mixing may also have been an issue, as the preformed solid could impede proper mixing. Furthermore, 30 grams of solidified metal were leftover in the LTM crucible after mixing and pouring into the mold, most likely the solid already formed in the LTM prior to mixing.

In summary, higher undercooling in $\Delta T_P = 80°C$ when compared to $\Delta T_P = 66°C$ causes a higher rate of nucleation, decreasing the average grain size and therefore increasing circularity. There is also a possibility that solid preformed in the LTM could act as additional nucleation sites. The correlation between grain size and circularity at *constant cooling rate* supports copious nucleation and solute impingement theory. None of the mechanistic theories in literature account for the correlation.

Figure 29 shows the effect of ΔT_P on the microstructure of Al-4.5%Cu cast by CDS. Grain size and circularity for each micrograph are presented in Table 15.

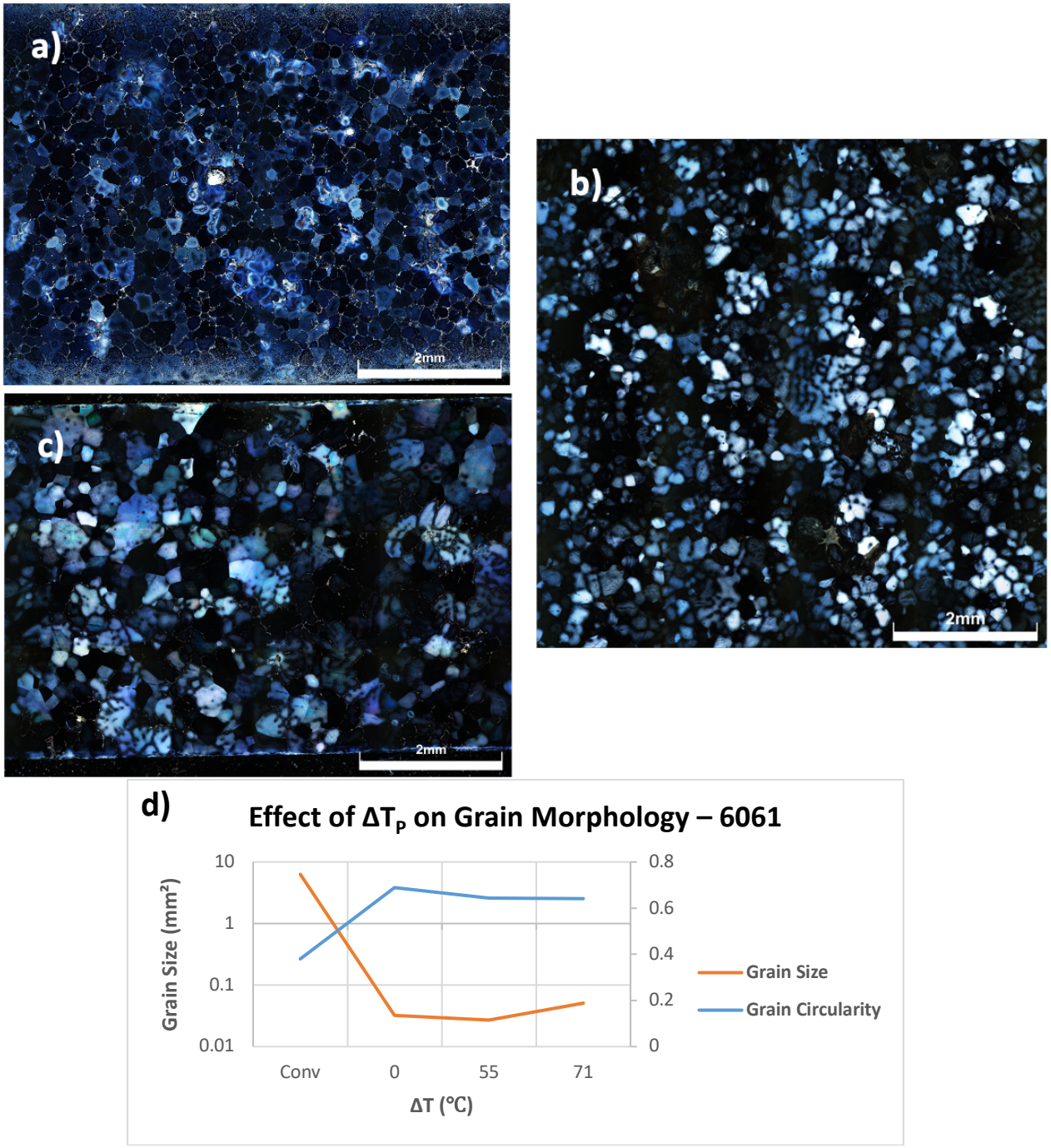


Figure 29: Anodized microstructure of 6061 cast by CDS with a ΔT_P of (a) 0°C, (b) 55°C, and (c) 71°C between precursor alloys accompanied by (d) the effect of variance of ΔT_P on morphology.

Table 15: Effect of differences in ΔT between precursor alloys on grain morphology in 6061.

ΔT_P (°C)	Precursor 2 (LTM) T (°C)	Cooling Rate (°C/s)	Avg. Grain Size (mm^2)	Grain Circularity
0	665	0.2	0.032	0.69
55	610	0.2	0.027	0.64
71	594	0.2	0.051	0.64

Figure 29 shows that the results of pouring 6061 by CDS with a ΔT_P of 0°C are very different from the results of its Al-4.5% counterpart. In fact, the grain size is comparable to CDS experiments with significant ΔT_P, and the circularity is the best achieved among all CDS experiments performed in this work. Cr in the HTM acts as a grain refiner, inducing icosahedral short-range ordering to form quasicrystals that nucleate FCC Al by heteroepitaxy [16].

6061 cast by CDS with a ΔT_P of 55°C, shown in Figure 29b represents the typical recipe for CDS with an LTM temperature just above its liquidus. Its grain size is similar to that of the ΔT_P of 0°C casting, but it has lower circularity. It also has a higher occurrence of the occasional large dendritic grain. Mixing will be discussed in detail in the next section, but it is evident that solute distribution at the macro scale is less homogenous when ΔT_P is 0°C. The reason that a ΔT_P of 0°C results in a higher circularity than a ΔT_P of 55°C may be that there is an abundance of unmixed Al-.2%Cr that can nucleate copiously at the onset of solidification. Solute elements such as Si and Mg can act to 'poison' the grain refining effect of Cr in Al [17], so it is possible that less efficient mixing is better, in this case.

A ΔT_P of 71°C should be approximately 25 percent solid in the LTM at the time of mixing. Quantitatively, it shows a slightly larger grain size than when ΔT_P is 55°C and the same grain circularity. Qualitatively, there is much more variance in the grain size. This suggests that preformed solids in the LTM prior to mixing are likely included in the resultant microstructure.

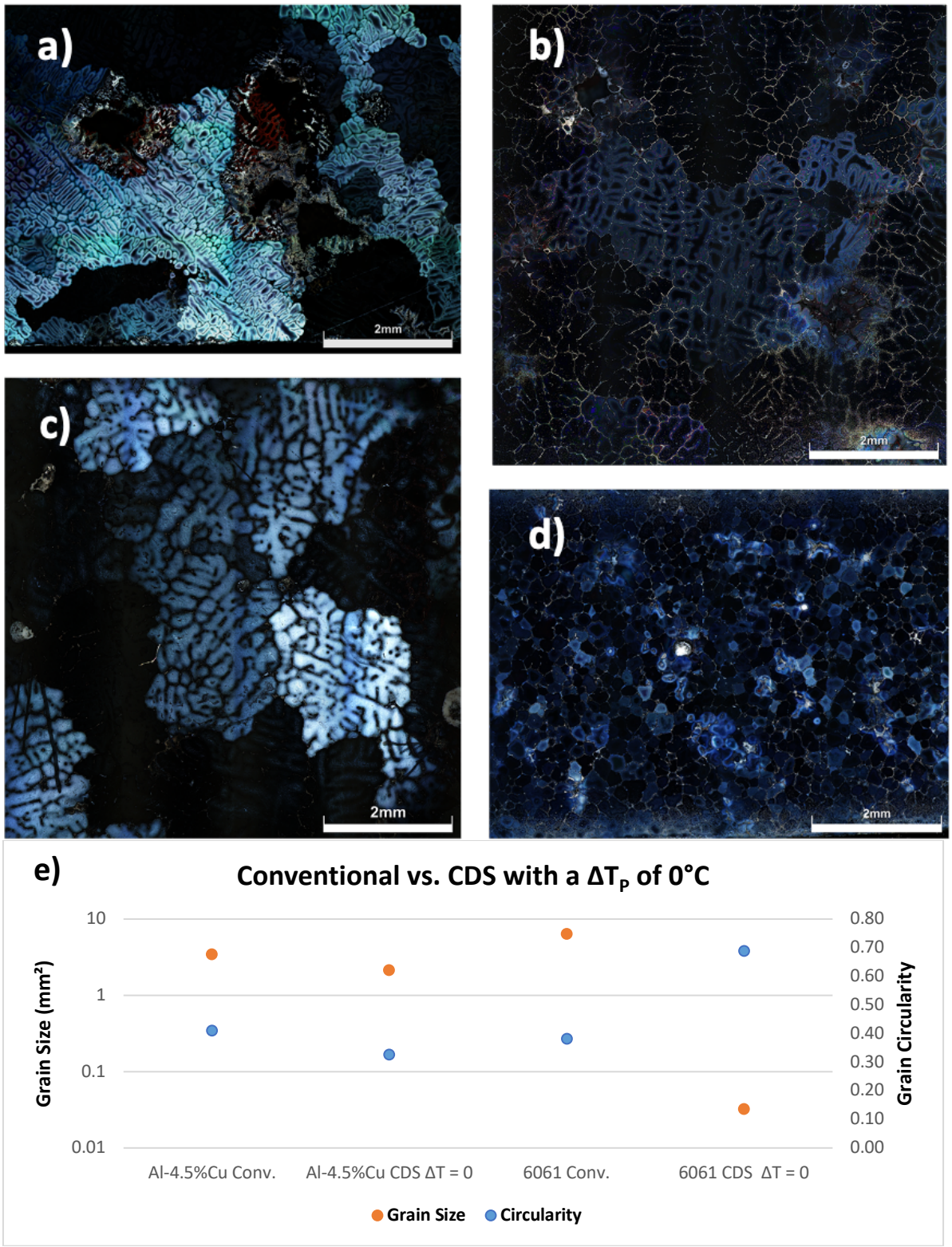


Figure 30: Comparison of (a) Al-4.5%Cu cast by conventional solidification against (b) CDS with a ΔT_P of 0°C and (c) 6061 cast by conventional solidification against (d) CDS with a ΔT_P of 0°C accompanied by (e) corresponding grain statistics.

Table 16: Conventional vs CDS with $\Delta T_P = 0°C$.

Casting	ΔT_P (°C)	Precursor 2 T (°C)	Cooling Rate (°C/s)	Avg. Grain Size (mm^2)	Grain Circularity
Conventional Al-4.5%Cu	-	-	0.2	3.443	0.41
CDS Al-4.5%Cu	0	665	0.2	2.14	0.33
Conventional 6061	-	-	0.2	6.31	0.38
CDS 6061	0	665	0.2	0.032	0.69

Figure 30 shows a comparison of Al-4.5%Cu and 6061, cast conventionally and by CDS with a $\Delta T_P = 0°C$. Al-4.5%Cu cast by CDS and conventionally share similar morphologies and large grain sizes. Tabulated data obtained from the micrographs are shown in Table 16. 6061 cast conventionally also exhibits similar large, dendritic microstructure. The standout is 6061 cast by CDS with a ΔT_P of 0°C. The conventional microstructures are standard for the respective alloys. Cr cannot act as a grain refiner in a homogenous melt of 6061 due to the aforementioned 'poisoning' of its grain refining properties by additional solute elements. The pure Al HTM precursor in the Al-4.5%Cu by CDS does not contain inherent grain refining inoculants, whereas the Al-.2%Cr HTM precursor in 6061 does. Figure 31 and Table 17 compare the 6061 CDS experiment with a ΔT_P of 0°C both with and without Cr in the HTM. They prove that the Cr acts as a grain refiner in the CDS process and especially when $\Delta T_P = 0°C$.

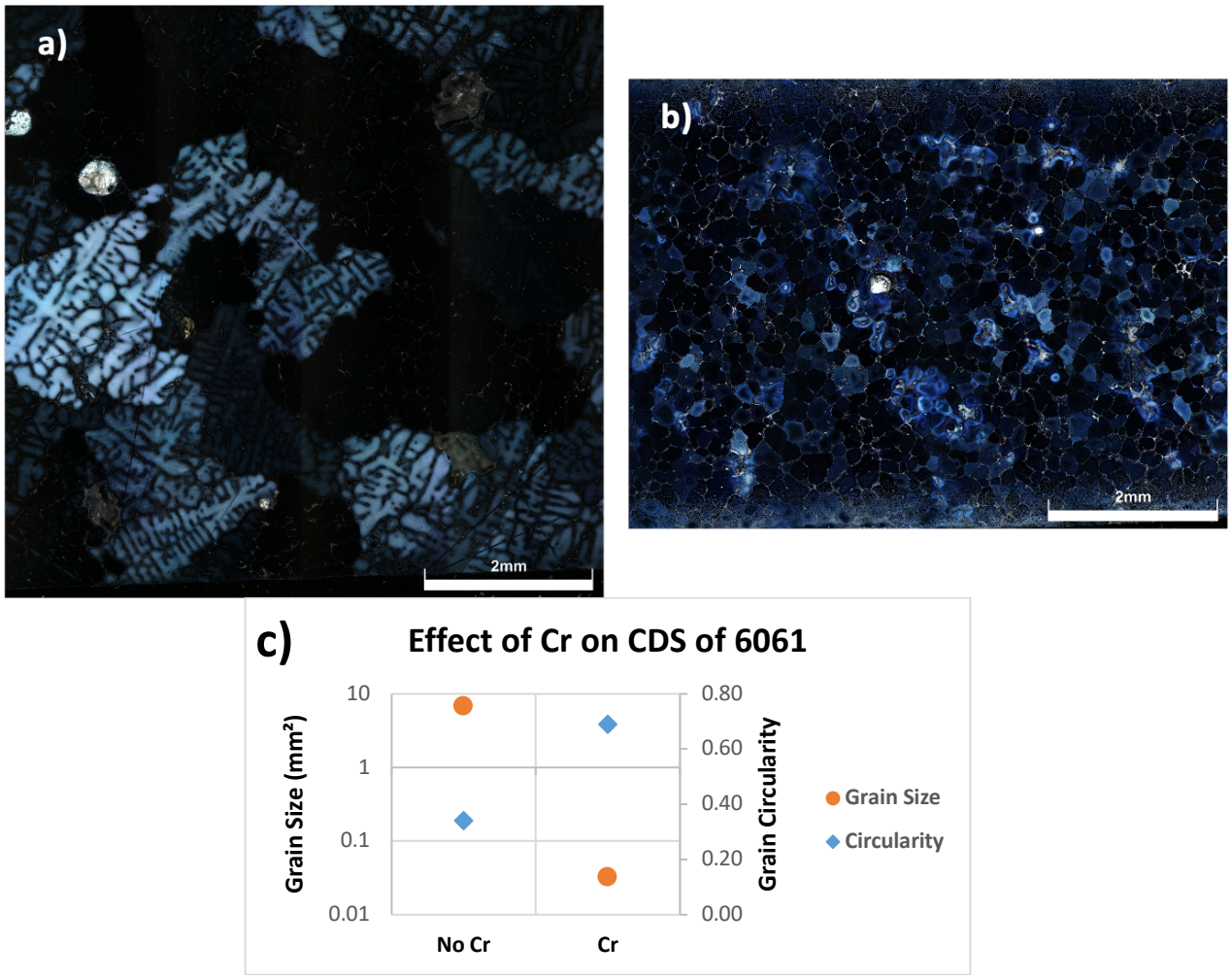


Figure 31: Comparison of AA6061 cast by Diffusion Solidification with a ΔT_P of 0°C both (a) without Cr and (b) with Cr accompanied by (c) corresponding grain statistics.

Table 17: Effect of Cr in the HTM.

Casting	ΔT_P (°C)	Precursor 2 (LTM) T (°C)	Cooling Rate (°C/s)	Avg. Grain Size (mm^2)	Grain Circularity
CDS 6061 w/o Cr	0	665	0.2	6.77	0.34
CDS 6061	0	665	0.2	0.032	0.69

In summary, there is a direct correlation between ΔT_P and grain size and morphology. A higher ΔT_P results in a more refined and circular microstructure unless there is an overabundance of preformed solid in the LTM. This is probably due to an increase in grain density resulting from a larger undercooling of the HTM, which supports the theory of copious nucleation as the

nucleation step in CDS. Further support comes from the 6061 study in which Cr in the HTM enacted copious nucleation even without a temperature differential. Current mechanistic theories of globular growth cannot explain the evident correlation between grain size and circularity in CDS alone, barring cooling rate changes or inoculant additions. Furthermore, mixing efficiency must play a role in the morphology of grains in the CDS process.

4.3 Effect of Mass Ratio and Mixing

The major factor delineating CDS from conventional casting is the mixing step. Figure 32 and Table 18 show the effect of mass ratio of HTM:LTM on grain size and morphology. A mass ratio of 4:1 produces slightly larger and less circular grains than one of 6.33:1. The likely reason is the ΔT_P difference, as discussed in the previous section.

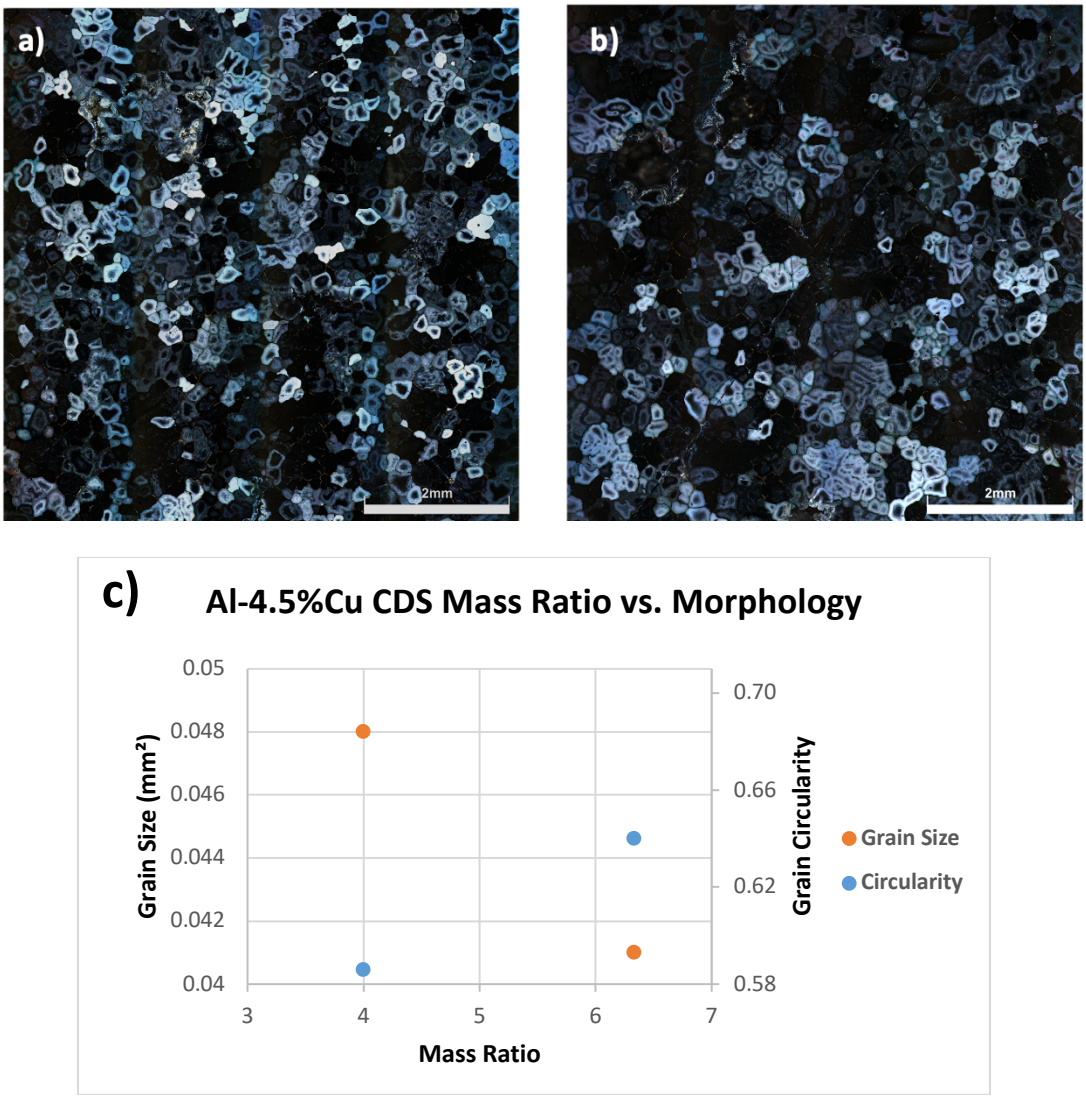


Figure 32: Microstructures of Al-4.5%Cu cast by CDS with mass ratios of (a) 6.33:1 and (b) 4:1 with (c) graphical representation of the contrast in morphology.

Table 18: Effect of mass ratio on grain size and morphology.

Precursor 1 (HTM) Comp.	Precursor 2 (LTM) Comp.	Mass Ratio of P1:P2	ΔT_P (°C)	T_L P1 (°C)	T_L P2 (°C)	Grain Size (mm^2)	Grain Circularity
Al	Al-33%Cu	6.33:1	112	660	548	.041	0.64
Al	Al-22.5%	4:1	66	660	594	.048	0.59

Figure 33 shows the effect that mass ratio and ΔT_P have on the relative standard deviation (RSD) of Cu content across a cross section of each respective sample. The procedure utilizing OES is detailed in the procedures section. RSD is used as a measure of the homogeneity of the

composition at the macro scale. A high RSD indicates poor mixing, while a low RSD indicates relatively better mixing.

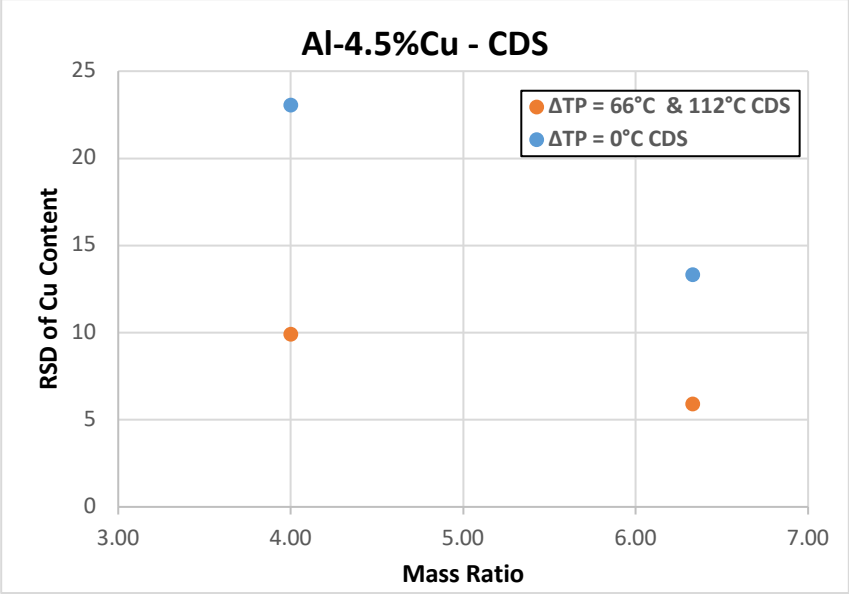


Figure 33: Effect of mass ratio and ΔT_P on mixing efficiency.

The results show that a higher mass ratio results in better mixing, and a ΔT_P of 0°C leads to worse mixing. The effect of mass ratio is somewhat intuitive: a larger momentum is interacting with a smaller mass, so the momentum diffusivity is higher. The effect of ΔT_P seems less intuitive. A ΔT_P of 0°C means no copious nucleation occurs to inhibit mixing, the melt is a higher temperature, which should increase convection. Lobasov and Shebeleva, however, observed that the larger the difference in temperature between two liquids being mixed, the greater the mixing efficiency [62]. The effect is confirmed again in the 6061 ΔT_P study shown in Table 19. This effect may actually be beneficial to the 6061 process, as poor mixing could prevent solute atoms from poisoning the grain refining effects of Cr in the HTM.

Table 19: Effect of ΔT_P on mixing efficiency in CDS of 6061

Element	Mg	Si	Cu	Cr
RSD ΔT_P = 0°C	7.64	9.13	11.85	3.62
RSD ΔT_P = 55°C	2.22	1.84	1.84	1.91

Table 20 shows the effect that a partially solidified LTM has on mixing efficiency. The trend without preformed solid is that higher ΔT_P results in better mixing efficiency, but the solid seems to negate the benefits entirely.

Table 20: Effect of solid preformed in the LTM on mixing efficiency.

Element	ΔT_P (°C)	Mass Ratio	Si	Fe	Cu
RSD 0% Solid in LTM	66	4	10.99	13.49	9.89
RSD 25% Solid in LTM	95	4	23.18	22.58	20.95

In summary, mechanical mixing is not completed simply by pouring. Momentum diffusivity can only achieve a fixed amount of mixing before it stalls. Atomic diffusion is the primary driving force for chemical equilibration beyond that. This would suggest that convection also falls off rapidly, which does not support the growth portion of the first mechanism detailed in section 2.2. Mixing efficiency is increased with increasing ΔT_P and with increasing mass ratio. Full chemical equilibration at the macro scale cannot be achieved by the current process, which might be beneficial to alloys with grain refining inoculants in the HTM. Even so, new mixing processes, such as the simultaneous pouring process used by Chen et al., will be necessary to upscale CDS [2].

4.3.1 Anomalous Grains

Figure 34 shows the microstructure of an Al-4.5%Cu cast in a steel mold by CDS. In the center is a large, so-called anomalous grain of pure Al, confirmed with an energy dispersive X-ray spectroscopy (EDS) line scan. It is surrounded by other such anomalous grains. Khalaf and Shankar studied the formation of these grains in detail and considered them in a three-step mechanism for nucleation and growth in CDS [40][41][42][43]. The casting in Figure 34 is one poured prior to full realization of an operating procedure. Early procedures neglected the stirring of the precursor alloys prior to the mixing step, detailed in Section 2.2.1. Once stirring of the Al-

33%Cu melt was added to the procedure, anomalous grains of pure aluminum no longer appeared in the microstructure of CDS castings. This suggests that the anomalous grains would have nucleated from low solute regions of the Al-33%Cu LTM caused by sedimentation of the copper solute as the temperature was lowered to 553°C. In short, the anomalous grains are likely a result of poor mixing practices *prior* to the mixing step of CDS.

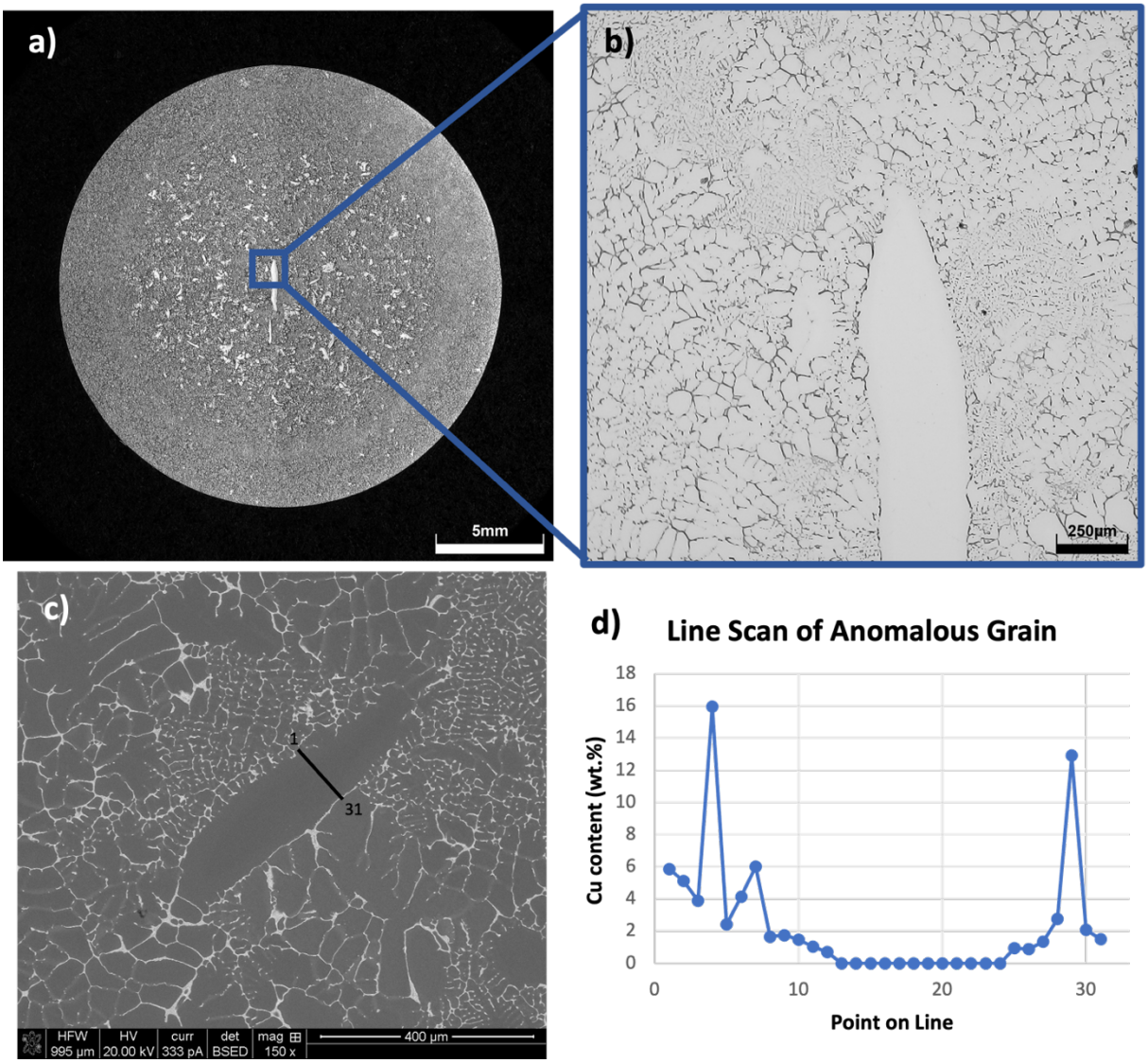


Figure 34: (a-b) Optical micrographs of an anomalous grains, (c) backscatter electron (BSE) image of the grain, and (d) EDS line scan of the grain.

4.4 Hot Tearing

Figure 35 shows the qualitative results of hot tearing tests of 6061 cast in sand molds conventionally and by CDS. Table 21 displays the measured compositions of the castings. The target composition was Al-1Mg-.6Si-.3Cu-.2Cr. The measured Si content in each was higher than expected. This is likely a result of a slightly higher amount of Al-Si master alloy than intended. Even so, all castings with the exception of Conv. 1 are within specification of 6061. The CDS tests showed a higher RSD than the conventional tests, further suggesting poor mixing efficiency in the CDS process.

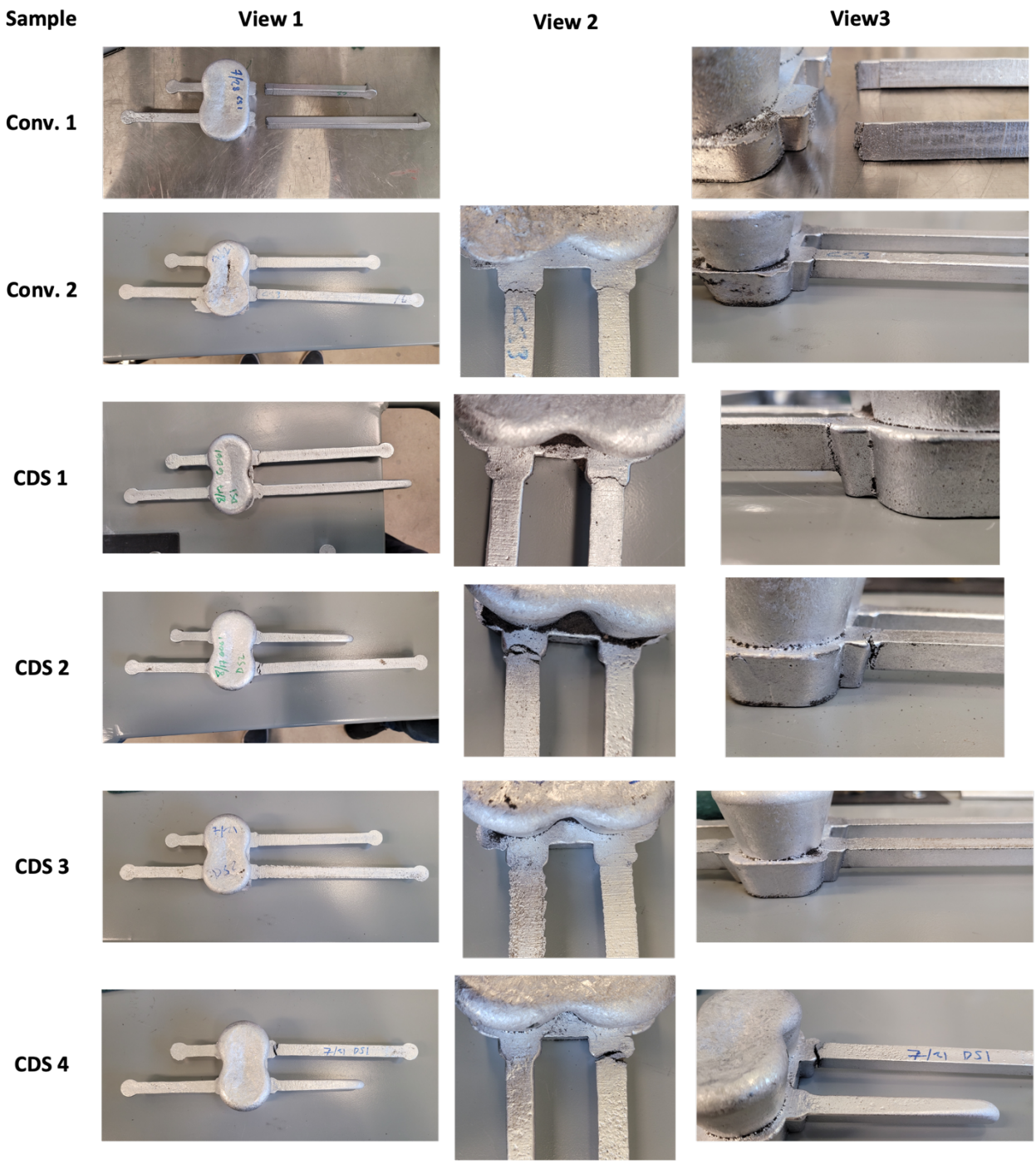


Figure 35: Hot tearing tests of 6061 cast in sand molds conventionally and by CDS.

Table 21: Measured compositions of 6061 hot tearing castings in sand molds.

		Si	Fe	Cu	Mg	Cr	Al
Conv. 1							
	Average (wt. %)	**0.855**	**0.0426**	**0.355**	**1.12**	**0.161**	**bal.**
	RSD	12.44	6.88	2.05	8.17	6.72	
Conv. 2							
	Average (wt. %)	**0.777**	**0.0424**	**0.330**	**1.14**	**0.182**	**bal.**
	RSD	2.84	9.26	2.59	2.89	1.91	
CDS 1							
	Average (wt. %)	**0.779**	**0.0378**	**0.293**	**0.894**	**0.179**	**bal.**
	RSD	16.96	24.57	14.19	11.58	4.40	
CDS 2							
	Average (wt. %)	**0.749**	**0.0442**	**0.328**	**1.00**	**0.173**	**bal.**
	RSD	12.99	15.70	16.07	12.39	6.93	
CDS 3							
	Average (wt. %)	**0.712**	**0.0434**	**0.319**	**1.01**	**0.207**	**bal.**
	RSD	8.85	13.51	11.79	7.77	3.92	
CDS 4							
	Average (wt. %)	**0.744**	**0.0429**	**0.301**	**0.993**	**0.264**	**bal.**
	RSD	19.96	12.30	9.04	7.22	4.14	

Hot tearing tests of conventional 6061 showed significant hot tearing at the base of each of the longer arms of the castings and no visible hot tearing in the shorter arms. The sample named Conv. 1 exhibited complete separation of the longer arms from the base of the casting. This complete separation occurred before the removal of the casting from the mold. Conv. 2 showed less severe, yet still significant, hot tearing. The crack formed on the longer arm was bigger than on the smaller arm.

Hot tear testing results for CDS were inconsistent. There were issues with filling that will be addressed in the next section. All CDS castings fully filled the shorter arms with no visible hot tearing. Table 22 ranks the castings in order of hot tearing severity and describes the cracking severity for each arm (only referring to the two longest arms).

Table 22: Hot tearing results listed from most severe hot tearing to least.

Most Severe	Casting	Short Arm Severity	Long Arm Severity
1	Conv. 1	Full breakaway	Full breakaway
2	CDS 4	Severe, initiated from two locations	No fill
3	CDS 2	No fill	Severe, initiated from two locations
4	Conv. 2	Moderate severity	Moderate severity
5	CDS 1	Moderate severity	No fill
6	CDS 3	Light severity, hairline	Light severity, hairline
Least Severe			

Figure 36 shows the microstructures of Conv. 1, CDS 1 and CDS 2. The microstructure of the conventional casting shows consistent and large dendritic grains with visibly low circularity. The grains are smaller than those from the conventional 6061 poured in a graphite mold, suggesting that the sand mold without a preheat enacted a faster cooling rate. CDS 1 contains large dendritic grains at the top corner of the sample but progressively more refined grains at the center. CDS 2 has refined grains *except* at the center. The large dendritic grains toward the center probably accounted for the severity of the hot tearing in CDS 2. In fact, rather than initiation at the sides of the arm, crack initiation in CDS 2 likely began at the center. The reason for the formation of dendritic grains in the CDS is unclear, though it is likely in part due to incomplete mixing detailed in section 3.4. This is especially likely given the significantly larger mass of the sand castings compared to all previous castings. Regardless, CDS 3 showed significantly lower hot tearing severity than either of the conventionally cast tests, nearly eliminating hot tearing altogether. However, there are still kinks to work out regarding mixing efficiency and fluidity if the process is to be utilized at the industrial scale.

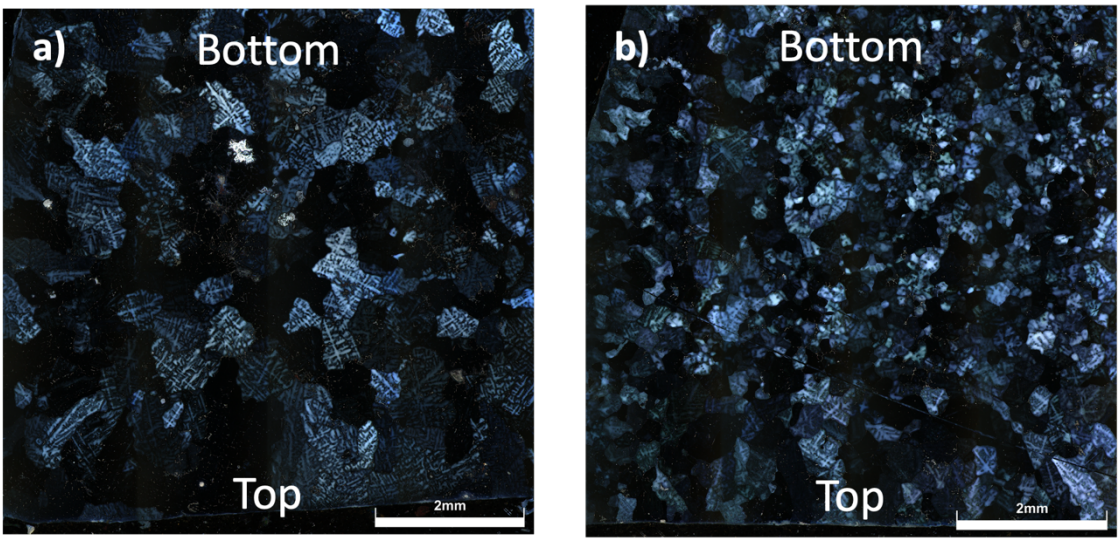


Figure 36: Microstructures (a) Conv. 1 and (b) CDS 1 hot tearing tests.

Figure 37 shows the results of hot tearing tests cast in a permanent tensile bar mold. Table 23 the results of the tests, which include casting defects and locations of hot tearing on tensile bars. Conventional 6061 had few problems filling the mold without casting defects, but invariably suffered from hot tears. Two CDS castings were free of hot tears, but only one was free of casting defects, namely cold shuts. Cold shuts result when two solidification fronts meet in a relatively cold melt and fail to fuse [63].

Table 23: Hot tearing and casting defects in 6061 cast conventionally and by CDS.

Sample	Hot Tear Location	Casting Defects
Conv. 1	Gauge	None
Conv. 2	Gauge	None
Conv. 3	Grip	Mild Cold Shut
Conv. 4	Grip	None
CDS 1	None	Moderate Cold Shut
CDS 2	Gauge	Severe Cold Shut
CDS 3	None	None
CDS 4	Gauge	None

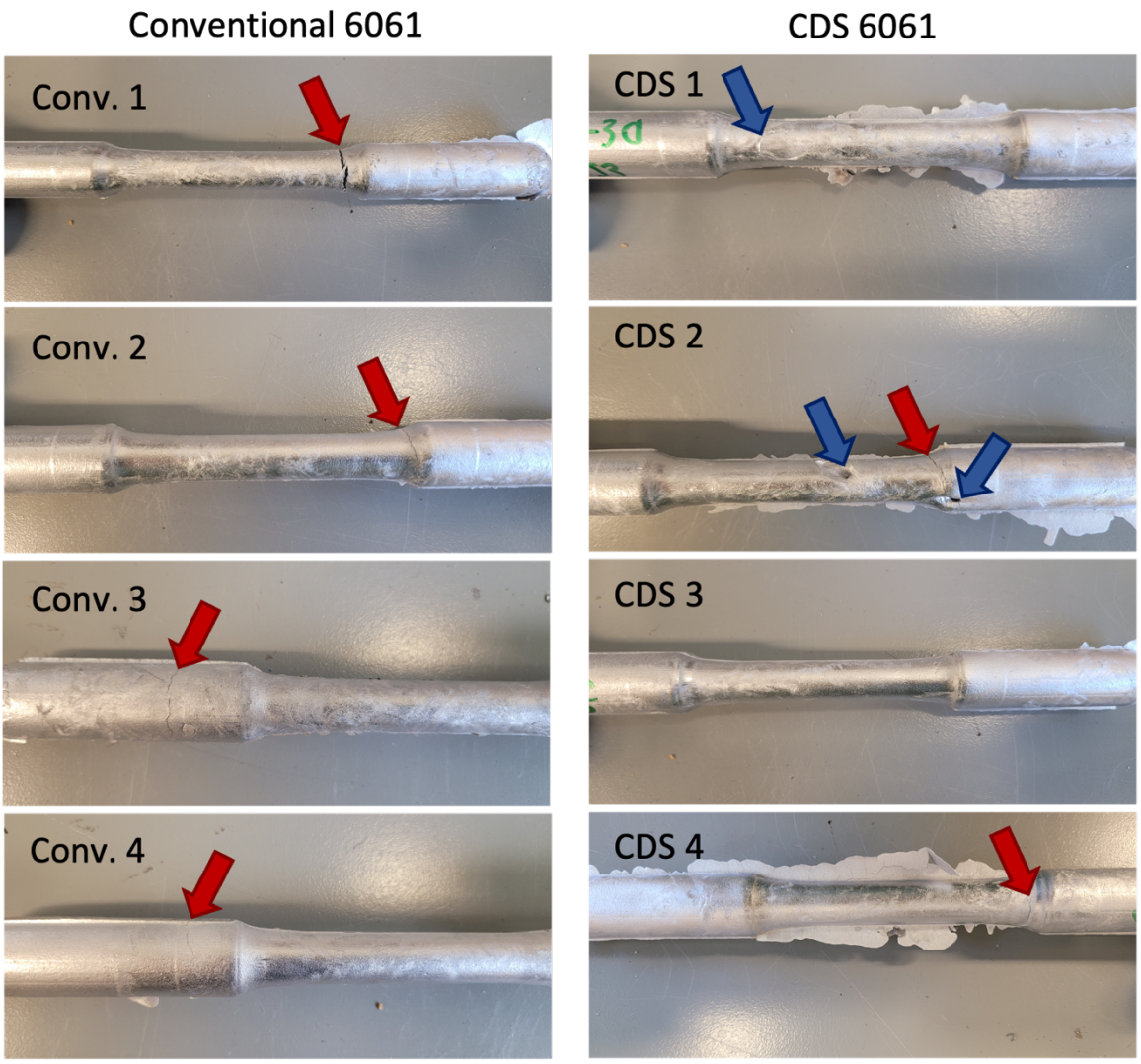


Figure 37: Conventionally and CDS cast 6061 hot tearing tests in a permanent tensile bar mold. Hot tears are indicated by red arrows, cold shuts by blue.

In summary, hot tearing were performed on 6061 cast conventionally and by CDS. Two types of molds, one sand and one steel, were used to observe hot tearing tendencies in different cooling regimes. All conventionally cast 6061 exhibited significant hot tearing, whereas one sand cast CDS sample showed only minor hot tearing and two cast in the permanent mold showed no hot tearing whatsoever. Unrefined dendritic grains in the microstructure were identified as a likely cause of hot tearing in CDS sand castings. These grains likely grew due to insufficient

mixing of precursor alloys and the relatively large volumes of the melts. Finally, CDS castings in both sand and steel molds faced severe issues with filling and fluidity.

4.5 Castability

Figure 38 shows examples of CDS castings with filling defects. In the sand castings, full fill was not achieved in some of the longer arms. In the steel, castings suffered from cold shuts. In conventional castings, defects such as these can be addressed with a sufficient superheat of the melt. Symeonidis et al. demonstrated that any superheat in the HTM would negate the benefits gained through CDS [35]. Functionally, CDS is a semi-solid metal (SSM) process. Solid has already formed in the resultant mixture before it even reaches the mold. Even the slightest cooling can initiate a significant amount of solidification. As a result, fluidity in alloys cast by CDS is low.

The castability of an aluminum alloys boils down to two factors: hot tearing susceptibility and fluidity. Both are serious issues facing wrought alloys, but fluidity is generally easier to compensate for with superheats or high pressure die casting. Hot tearing can only be resolved by changing the composition of the alloy or refining its grains. Grain refiners and SSMs besides CDS that target hot tearing come with several issues, some of which CDS can resolve. However, it is evident that much of the ground gained in castability by reducing hot tearing is lost again by also reducing fluidity. CDS cannot be superheated, so high pressure die casting may be the only casting process for which CDS is suited.

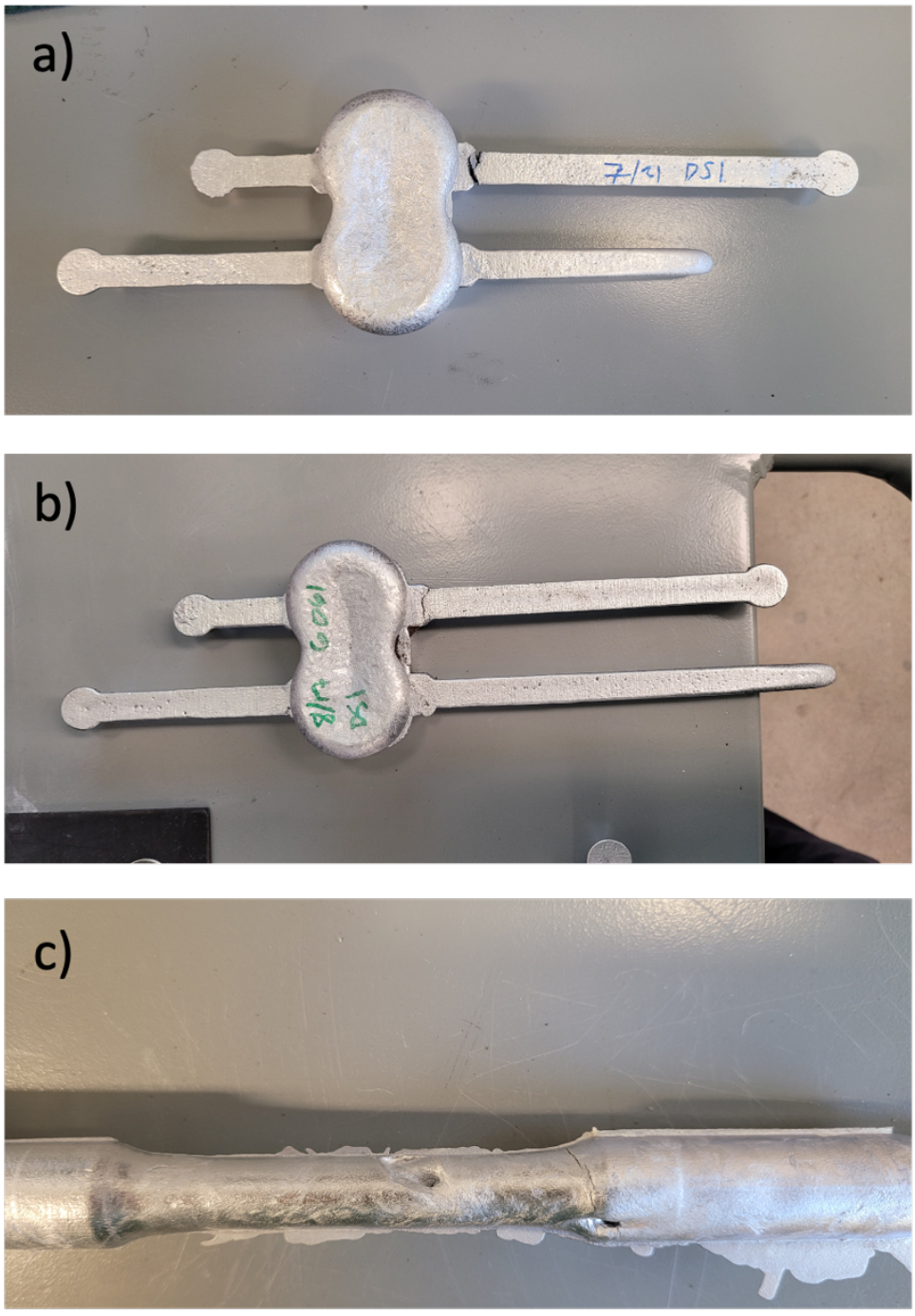


Figure 38: CDS castings of 6061 with significant pouring defects.

Chapter 5: Conclusions

The effectiveness of Controlled Diffusion Solidification in producing castings with refined, globular grains was confirmed. The influence of various parameters including cooling rate, temperature differential between precursors, and mass ratio on the extent of grain refinement and circularity in Al-4.5%Cu and 6061 alloys cast by CDS were examined. Observations made under various parameter conditions not only raised questions about the fundamental mechanisms driving CDS but also contributed to the formulation of a new mechanistic theory. Finally, the castability of 6061 cast by CDS was evaluated by examining trends in hot tearing and fluidity. The following conclusions were drawn:

- Grain refining effects of CDS and high cooling rate are compounded, producing smaller grains than either method can produce alone. CDS has a greater positive effect on grain circularity than cooling rate. When combined, circularity decreases compared to CDS alone. This effect cannot be sufficiently explained by the current theories on growth of globular grains.
- The magnitude of the temperature differential between precursor alloys, ΔT_P, is directly correlated to grain size and morphology in CDS. A higher ΔT_P results in smaller and more circular grains. This is a result of larger undercooling in the HTM upon mixing, which results in higher grain density. The correlation of grain density and grain circularity at constant cooling rate also does not mesh with current theories.
- Cr in a high purity Al HTM acts as a grain refiner, resulting in a refined and globular microstructure, even when $\Delta T_P = 0°C$. There may be avenues for pouring 6061 at higher temperatures to address fluidity issues associated with CDS.

- Momentum diffusivity during the mixing method used in this and almost every other study of CDS is not sufficient to chemically equilibrate the resultant liquid even at the macro scale. New methods of mixing the two precursors are desperately needed to progress development of the CDS process.
- Hot tearing tests showed that 6061 cast by CDS could exhibit reduced hot tearing susceptibility, but poor mixing exacerbated by large volume castings made the successes inconsistent.
- Castability is qualified by both hot tearing susceptibility and fluidity. CDS is a semi-solid metal process (SSM) that can significantly reduce hot tearing tendencies in wrought alloys but pays the price in fluidity. Alternative routes to refined microstructure, such as Cr inoculates in a superheated HTM will be necessary moving forward. Otherwise, the only suitable casting process for CDS is likely to be high pressure die casting, as it is with other SSMs.
- Based on a review of literature and results of experimentation, an updated framework to explain the mechanisms by which CDS promotes the formation of refined and globular grains is proposed:
    1. Copious nucleation: Undercooling of the high thermal mass liquid (HTM) upon thermal equilibration promotes copious nucleation at the interface between the HTM and low thermal mass liquid (LTM). The addition of grain refiners in the HTM can increase the density of forming nuclei. Latent heat of fusion released from the forming nuclei stymie their growth.
    2. Chemical equilibration: Mixing and atomic diffusion ensure that solute rich liquid surround nuclei. High mixing efficiency will make this more homogenous.

3. Unconstrained growth: Nuclei will grow conventionally as the functionally homogenous melt cools, forming equiaxed dendrites. Expulsion of solute ahead of the dendrites will form boundary layers of enriched liquid, also called solute fields.
4. Solute field impingement: The high density of grains will result in impingement of solute fields as grains grow close to each other. Further enrichment of these impinged solute fields will eliminate constitutional undercooling ahead of the solid-liquid interface.
5. Slow growth: With the assumption of a near isothermal melt in the local impinged solute field, the driving force for solidification of the primary becomes curvature undercooling. Curvature undercooling works to minimize the excess energy associated with the solid-liquid interface, resulting in a ‘smoothing’ of dendritic features. The result is a globular or rosette microstructure.

Chapter 6: Future Work

Fluidity was a significant issue while creating castings of 6061 by CDS. Full fill of sand molds was successful only one out of four attempts. Normally, there is no option in CDS for superheat. However, the 6061 casting when ΔT_P was 0°C showed promise for casting CDS above the liquidus of at least the LTM. Future work would be negligent not to test the upper limits of superheat in both HTM and LTM in the 6061 system, given that Cr can act as a grain refiner.

The natural follow-up to such tests would be the development of heat treatments for 6061 cast by CDS. The composition of the interdendritic liquid at the time of solidification could be different than convention due to the presegregation of solute inherent to the process. Once optimum heat treatment is established, tensile properties should be obtained. It will be important to know if the 6061 cast by CDS can outperform cast alloys with similar uses such as A356. Naturally, it should also be compared to wrought 6061.

Mixing efficiency was found in this study to be too low for full chemical equilibration on the macro scale. As such, macroscale compositional mappings of the samples should be compared to respective microstructures to observe the effects of fluctuating solute concentrations. Mixing techniques such as simultaneous mixing, outlined in section 6.4, should also be observed for mixing efficiency. Its potential for large CDS castings is far greater than that of other current methods, as evidenced by this work.

While the grain density theory listed above is supported by evidence, more work should be dedicated to proving or disproving it. Clarification of the mechanisms of CDS is still needed for its advancement to use in the industrial setting.

References

[1] Ghiaasiaan, R., & Shankar, S. (2020). Microstructure, Intermetallic Phases, and Fractography of the Cast Al-5.8Zn-2.2Mg-2.5Cu Alloy by Controlled Diffusion Solidification. *Metallurgical and Materials Transactions A*, *51*(9), 4711–4726. https://doi.org/10.1007/s11661-020-05885-z

[2] Chen, T. J., Yang, X. K., Xue, H., Bi, G. L., Zhang, X. Z., & Guan, R. G. (2022). Mixing process and nucleation of an Al-Si alloy during controlled diffusion solidification with simultaneous mixing and effect of mixing rate. *Journal of Materials Science*, *57*(4), 3018–3040. https://doi.org/10.1007/s10853-021-06730-3

[3] Polmear, Ian, David StJohn, Jian-Feng Nie, and Ma Qian. *Light Alloys: Metallurgy of the Light Metals*. Butterworth-Heinemann, 2017.

[4] Sigworth, GK. "Hot Tearing of Metals." *TRANSACTIONS-AMERICAN FOUNDRYMENS SOCIETY*, 1996, 1053–62.

[5] Li, Shimin, Diran Apelian, and Kumar Sadayappan. "Hot Tearing in Cast Aluminum Alloys." *Materials Science Forum* 690 (June 2011): 355–58. https://doi.org/10.4028/www.scientific.net/MSF.690.355.

[6] Campbell, John. *Castings*. Elsevier, 2003.

[7] Li, S., and D. Apelian. "Hot Tearing of Aluminum Alloys: A Critical Literature Review." *International Journal of Metalcasting* 5, no. 1 (January 2011): 23–40. https://doi.org/10.1007/BF03355505.

[8] Rappaz, M., J. -M. Drezet, and M. Gremaud. "A New Hot-Tearing Criterion." *Metallurgical and Materials Transactions A* 30, no. 2 (February 1999): 449–55. https://doi.org/10.1007/s11661-999-0334-z.

[9] Akhyar, H., V. Malau, Suyitno, and P.T. Iswanto. "Hot Tearing Susceptibility of Aluminum Alloys Using CRCM-Horizontal Mold." *Results in Physics* 7 (2017): 1030–39. https://doi.org/10.1016/j.rinp.2017.02.041.

[10] Porter, David A, and Kenneth E Easterling. *Phase Transformations in Metals and Alloys (Revised Reprint)*. CRC press, 2009.

[11] Flemings, Merton C. "Solidification Processing." *Metallurgical and Materials Transactions B* 5 (1974): 2121–34.

[12] Zeng, Xiaochun, Cassandra Ferguson, Kumar Sadayappan, and Sumanth Shankar. "Effect of Titanium Levels on the Hot Tearing Sensitivity and Abnormal Grain Growth After T4 Heat Treatment of Al–Zn–Mg–Cu Alloys." *International Journal of Metalcasting* 12, no. 3 (July 2018): 457–68. https://doi.org/10.1007/s40962-018-0227-2.

[13] Greer, A.L, A.M Bunn, A Tronche, P.V Evans, and D.J Bristow. "Modelling of Inoculation of Metallic Melts: Application to Grain Refinement of Aluminium by Al–Ti–B." *Acta Materialia* 48, no. 11 (June 2000): 2823–35. https://doi.org/10.1016/S1359-6454(00)00094-X.

[14] McCartney, D. G. "Grain Refining of Aluminium and Its Alloys Using Inoculants." *International Materials Reviews* 34, no. 1 (January 1989): 247–60. https://doi.org/10.1179/imr.1989.34.1.247.

[15] Fan, Z., F. Gao, Y. Wang, H. Men, and L. Zhou. "Effect of Solutes on Grain Refinement." *Progress in Materials Science* 123 (January 2022): 100809. https://doi.org/10.1016/j.pmatsci.2021.100809.

[16] Rappaz, Michel, and Güven Kurtuldu. “Thermodynamic Aspects of Homogeneous Nucleation Enhanced by Icosahedral Short Range Order in Liquid Fcc-Type Alloys.” *JOM* 67, no. 8 (August 2015): 1812–20. https://doi.org/10.1007/s11837-015-1328-5.

[17] Arjuna Rao, A., B. S. Murty, and M. Chakraborty. “Influence of Chromium and Impurities on the Grain- Refining Behavior of Aluminum.” *Metallurgical and Materials Transactions A* 27, no. 3 (March 1996): 791–800. https://doi.org/10.1007/BF02648967.

[18] Agboola, Joseph B, Reyaz H Khan, and Samson O Ubokwe. “Effect of Chromium on Grain Refinement of LM11 Aluminium Alloy Sand Castings.” *FUOYE Journal of Engineering and Technology* 2, no. 1 (March 31, 2017). https://doi.org/10.46792/fuoyejet.v2i1.47.

[19] Wang, Xuan, Pin-Kui Ma, Zhao-Yuan Meng, Shao-You Zhang, Xu Liu, Cheng Wang, and Hui-Yuan Wang. “Effect of Trace Cr Alloying on Centerline Segregations in Sub-Rapid Solidified Al–Mg–Si (AA6061) Alloys Fabricated by Twin-Roll Casting.” *Materials Science and Engineering: A* 825 (September 2021): 141896. https://doi.org/10.1016/j.msea.2021.141896.

[20] Flemings, M. C., R. G. Riek, and K. P. Young. “Rheocasting.” *Materials Science and Engineering* 25 (1976): 103–17.

[21] Scamans, G, and Z Fan. “Rheoforming of Novel Aluminium and Magnesium Alloys.” *Aluminium International Today* 17, no. 6 (December 2005): 22-22,24,26.

[22] Easton, M. A., M. Qian, A. Prasad, and D. H. StJohn. “Recent Advances in Grain Refinement of Light Metals and Alloys.” *Current Opinion in Solid State and Materials Science* 20, no. 1 (2016): 13–24. https://doi.org/10.1016/j.cossms.2015.10.001.

[23] Wannasin, J., S. Janudom, T. Rattanochaikul, R. Canyook, R. Burapa, T. Chucheep, and S. Thanabumrungkul. “Research and Development of Gas Induced Semi-Solid Process for Industrial Applications.” *Transactions of Nonferrous Metals Society of China* 20 (September 2010): s1010–15. https://doi.org/10.1016/S1003-6326(10)60622-X.

[24] Langford, George, and Robert E Cunningham. “Steel Casting by Diffusion Solidification.” *METALLURGICAL TRANSACTIONS B*, n.d.

[25] Langford, G, and D Apelian. “Diffusion Solidification.” *JOM* 32 (1980): 28–33.

[26] Saha, D., Shankar, S., Apelian, D., & Makhlouf, M. M. (2004). Casting of aluminum-based wrought alloys using controlled diffusion solidification. *Metallurgical and Materials Transactions A*, *35*(7), 2174–2180. https://doi.org/10.1007/s11661-004-0167-8

[27] Animasaun, Isaac Lare, Nehad Ali Shah, Abderrahim Wakif, Basavarajappa Mahanthesh, Ramachandran Sivaraj, and Olubode Kolade Koríko. *Ratio of Momentum Diffusivity to Thermal Diffusivity: Introduction, Meta-Analysis, and Scrutinization*. CRC Press, 2022.

[28] Zhang, Fan, Yong Du, Shuhong Liu, and Wanqi Jie. “Modeling of the Viscosity in the AL–Cu–Mg–Si System: Database Construction.” *Calphad* 49 (June 2015): 79–86. https://doi.org/10.1016/j.calphad.2015.04.001.

[29] Brandt, R., and G. Neuer. “Electrical Resistivity and Thermal Conductivity of Pure Aluminum and Aluminum Alloys up to and above the Melting Temperature.” *International Journal of Thermophysics* 28, no. 5 (November 7, 2007): 1429–46. https://doi.org/10.1007/s10765-006-0144-0.

[30] Giordanengo, B., N. Benazzi, J. Vinckel, J.G. Gasser, and L. Roubi. "Thermal Conductivity of Liquid Metals and Metallic Alloys." *Journal of Non-Crystalline Solids* 250–252 (August 1999): 377–83. https://doi.org/10.1016/S0022-3093(99)00268-9.

[31] Apelian, D., Makhlouf, M. M., & Saha, D. (2006). CDS Method for Casting Aluminium-Based Wrought Alloy Compositions: Theoretical Framework. *Materials Science Forum*, *519–521*, 1771–1776. https://doi.org/10.4028/www.scientific.net/MSF.519-521.1771

[32] Cini, E., Vinet, B., & Desré, P. J. (2000). A thermodynamic approach to homogeneous nucleation via fluctuations of concentration in binary liquid alloys. *Philosophical Magazine A*, *80*(4), 955–966. https://doi.org/10.1080/01418610008212092

[33] Das, A., S. Ji, and Z. Fan. "Morphological Development of Solidification Structures under Forced Fluid Flow: A Monte-Carlo Simulation." *Acta Materialia* 50, no. 18 (October 2002): 4571–85. https://doi.org/10.1016/S1359-6454(02)00305-1.

[34] Wu, Shusen, Xueping Wu, and Zehui Xiao. "A Model of Growth Morphology for Semi-Solid Metals." *Acta Materialia* 52, no. 12 (July 2004): 3519–24. https://doi.org/10.1016/j.actamat.2004.04.005.

[35] Symeonidis, K., Apelian, D., & Makhlouf, M. M. (n.d.). *CONTROLLED DIFFUSION SOLIDIFICATION*.

[36] Symeonidis, K. (n.d.). *The Controlled Diffusion Solidification Process: Fundamentals and Principles*.

[37] Apelian, D., & Saha, D. (n.d.). *NOVEL AND ADVANCED SOLIDIFICATION PROCESSES FOR THE MANUFACTURE OF HIGH INTEGRITY ALUMINUM CAST COMPONENTS*.

[38] Khalaf, A. A., Ashtari, P., & Shankar, S. (2009). Formation of Nondendritic Primary Aluminum Phase in Hypoeutectic Alloys in Controlled Diffusion Solidification (CDS): A Hypothesis. *Metallurgical and Materials Transactions B*, *40*(6), 843–849. https://doi.org/10.1007/s11663-009-9285-4

[39] Ghiaasiaan, R., Shankar, S., & Apelian, D. (n.d.). *Control Diffusion Solidification (CDS): An Overview of Mechanism and Application*.

[40] Khalaf, A. A., & Shankar, S. (2011). Favorable Environment for a Nondendritic Morphology in Controlled Diffusion Solidification. *Metallurgical and Materials Transactions A*, *42*(8), 2456–2465. https://doi.org/10.1007/s11661-011-0641-z

[41] Khalaf, A. A., & Shankar, S. (2012). Effect of mixing rate on the morphology of primary Al phase in the controlled diffusion solidification (CDS) process. *Journal of Materials Science*, *47*(23), 8153–8166. https://doi.org/10.1007/s10853-012-6711-9

[42] Khalaf, A. A. A. (n.d.). *Controlled Diffusion Solidification: Process Mechanism and Parameter Study*.

[43] Khalaf, A. A., & Shankar, S. (2020). Mechanism of Anomalous Grain Formation During Controlled Diffusion Solidification. *JOM*, *72*(11), 3733–3743. https://doi.org/10.1007/s11837-020-04198-1

[44] Pourgharibshahi, M., Saghafian, H., Divandari, M., & Timelli, G. (2019). Controlled Diffusion Solidification Pathway of an AA 7xxx Series Aluminum Alloy. *Metallurgical and Materials Transactions A*, *50*(1), 326–335. https://doi.org/10.1007/s11661-018-5000-x

[45] Ghiaasiaan, R., Zeng, X., & Shankar, S. (2014). Controlled Diffusion Solidification (CDS) of Al-Zn-Mg-Cu (7050): Microstructure, heat treatment and mechanical

properties. *Materials Science and Engineering: A*, *594*, 260–277. https://doi.org/10.1016/j.msea.2013.11.087

[46] Khalaf, A. A. (2022). Studying of Non-Dendritic Microstructure Forming in Controlled Diffusion Solidification. *International Journal of Metalcasting*, *16*(1), 223–233. https://doi.org/10.1007/s40962-021-00590-y

[47] Yang, X., Li, Y., Luo, X., Zhou, H., Cai, Q., Li, M., & Ma, Y. (2019). Microstructural evaluation and mechanical properties of 7075 aluminum alloy prepared by controlled diffusion solidification. *China Foundry*, *16*(4), 238–247.

[48] Birsan, G. (2009). Shaped casting of aluminum wrought alloys by controlled diffusion solidification (CDS) in a tilt-pour gravity casting process. *McMaster University*.

[49] Ashtari, P., Birsan, G., Khalaf, A., & Shankar, S. (2011). Controlled Diffusion Solidification of 2024, 6082 and 7075 Al Alloys via Tilt-Pour Casting Process. *International Journal of Metalcasting*, *5*(2), 43–64. https://doi.org/10.1007/BF03355471

[50] Saha, D., Shankar, S., Apelian, D., & Makhlouf, M. M. (n.d.). *CONTROLLED DIFFUSION SOLIDIFICATION – MANUFACTURING NET SHAPED AL BASED WROUGHT ALLOY*.

[51] Seyed, R. G. (n.d.). PhD Thesis-S. Reza Ghiaasiaan. McMaster University-Mechanical Engineering. *Mechanical Engineering*.

[52] Pourgharibshahi, M., Divandari, M., Saghafian Larijani, H., & Ashtari, P. (2017). Controlled diffusion solidification processing: A review. *Journal of Materials Processing Technology*, *250*, 203–219. https://doi.org/10.1016/j.jmatprotec.2017.07.018

[53] Aluminum Association. "TealSheet.Pdf," 2018.

[54] Easton, M.A., and D.H. StJohn. "Improved Prediction of the Grain Size of Aluminum Alloys That Includes the Effect of Cooling Rate." *Materials Science and Engineering: A* 486, no. 1–2 (July 2008): 8–13. https://doi.org/10.1016/j.msea.2007.11.009.

[55] Liang, Guofang, Yahia Ali, Guoqiang You, and Ming-Xing Zhang. "Effect of Cooling Rate on Grain Refinement of Cast Aluminium Alloys." *Materialia* 3 (November 2018): 113–21. https://doi.org/10.1016/j.mtla.2018.08.008.

[56] Shankar, S., Saha, D., Apelian, D., & Makhlouf, M. M. (n.d.). *CDS: CONTROLLED DIFFUSION SOLIDIFICATION*.

[57] Ashtari, P., Birsan, G., & Shankar, S. (2009). *Favorable alloy compositions and melt temperatures to cast 2XXX and 7XXX Al alloys by controlled diffusion solidification (CDS)*. 223–230.

[58] B07 Committee. "Specification for Aluminum-Alloy Permanent Mold Castings." ASTM International. Accessed September 21, 2023. https://doi.org/10.1520/B0108_B0108M-19.

[59] Vander Voort, G, and Elena P Manilova. "Metallographic Etching of Aluminum and Its Alloys." *Buehler Ltd, EUA*, 2009.

[60] Crawford, Alastair. "Understanding Fire Histories: The Importance of Charcoal Morphology," 2015.

[61] Liang, Guofang, Yahia Ali, Guoqiang You, and Ming-Xing Zhang. "Effect of Cooling Rate on Grain Refinement of Cast Aluminium Alloys." *Materialia* 3 (November 2018): 113–21. https://doi.org/10.1016/j.mtla.2018.08.008.

[62] Lobasov, A S, and A A Shebeleva. “Initial Temperatures Effect on the Mixing Efficiency and Flow Modes in T-Shaped Micromixer.” *Journal of Physics: Conference Series* 899 (September 2017): 022010. https://doi.org/10.1088/1742-6596/899/2/022010.

[63] Rao, P.N. *Manufacturing Technology*. McGraw Hill Education, 2013. https://books.google.com/books?id=fSHZAgAAQBAJ.